


# The allosteric interplay between S-nitrosylation and glycine binding controls the activity of human serine racemase

Francesco Marchesani<sup>1</sup>, Eleonora Gianquinto<sup>2</sup>, Ida Autiero<sup>3,4</sup>, Annalisa Michielon<sup>1</sup>, Barbara Campanini<sup>1</sup>, Serena Faggiano<sup>1,5</sup>, Stefano Bettati<sup>5,6</sup>, Andrea Mozzarelli<sup>1,5</sup>, Francesca Spyarakis<sup>2</sup> and Stefano Bruno<sup>1</sup> 

<sup>1</sup> Dipartimento di Scienze degli Alimenti e del Farmaco, Università degli Studi di Parma, Italy

<sup>2</sup> Dipartimento di Scienza e Tecnologia del Farmaco, Università degli Studi di Torino, Italy

<sup>3</sup> Molecular Horizon Srl, Bettona, PG, Italy

<sup>4</sup> Consiglio Nazionale delle Ricerche, Istituto di Biostrutture e Bioimmagini, Napoli, Italy

<sup>5</sup> Consiglio Nazionale delle Ricerche, Istituto di Biofisica, Pisa, Italy

<sup>6</sup> Dipartimento di Medicina e Chirurgia, Parma, Italy

## Keywords

allosteric modulation; D-serine; fluorescence spectroscopy; glycine; molecular dynamics; nitrosylation; NMDA receptors; pyridoxal phosphate; serine racemase

## Correspondence

S. Bruno, Area Parco delle Scienze 27/A,  
43124 Parma, Italy  
Tel: +390521906613  
E-mail: stefano.bruno@unipr.it  
F. Spyarakis, Via Pietro Giuria 9, 10125  
Torino, Italy  
Tel: + 390116707185  
E-mail: francesca.spyarakis@unito.it

Francesco Marchesani and Eleonora  
Gianquinto contributed equally to the work

(Received 24 September 2020, revised 6  
November 2020, accepted 9 November  
2020)

doi:10.1111/febs.15645

Human serine racemase (hSR) catalyzes the biosynthesis of D-serine, an obligatory co-agonist of the NMDA receptors. It was previously found that the reversible S-nitrosylation of Cys113 reduces hSR activity. Here, we show by site-directed mutagenesis, fluorescence spectroscopy, mass spectrometry, and molecular dynamics that S-nitrosylation stabilizes an open, less-active conformation of the enzyme. The reaction of hSR with either NO or nitroso donors is conformation-dependent and occurs only in the conformation stabilized by the allosteric effector ATP, in which the  $\epsilon$ -amino group of Lys114 acts as a base toward the thiol group of Cys113. In the closed conformation stabilized by glycine—an active-site ligand of hSR—the side chain of Lys114 moves away from that of Cys113, while the carboxyl side-chain group of Asp318 moves significantly closer, increasing the thiol pK<sub>a</sub> and preventing the reaction. We conclude that ATP binding, glycine binding, and S-nitrosylation constitute a three-way regulation mechanism for the tight control of hSR activity. We also show that Cys113 undergoes H<sub>2</sub>O<sub>2</sub>-mediated oxidation, with loss of enzyme activity, a reaction also dependent on hSR conformation.

## Introduction

S-nitrosylation is a cysteine post-translational modification that reversibly regulates protein function [1,2]. It results from either the transnitrosylation by S-

nitrosoglutathione (GSNO) [2] or S-nitrosylated proteins [3]. Alternatively, nitrogen monoxide (NO) produced by nitric oxide synthases (NOSs) can react

## Abbreviations

DAAO, D-amino acid oxidase; ED, essential dynamics; GSNO, S-nitrosoglutathione; HRP, horseradish peroxidase; hSR, human serine racemase; LDH, lactate dehydrogenase; MAHMA NO<sub>2</sub>oate, (Z)-1-[N-methyl-N-[6-(N-methylammoniohexyl)amino]]diazene-1-ium-1,2-diolate; MD, molecular dynamics; MLI, malonate; NO, nitrogen monoxide; NOS, nitric oxide synthase; PCA, principal component analysis; PLP, pyridoxal 5'-phosphate; RMSD, root-mean-square deviation; RMSF, root-mean-square fluctuation; SR, serine racemase; WT, wild type.

directly with cysteine residues, forming an unstable intermediate that undergoes O<sub>2</sub>-mediated oxidation to S-nitrosocysteines [1]. The latter mechanism constitutes both an intracellular and a paracrine signaling pathway, as NO can diffuse out of the generating cell and reach nearby target cells.

Regulation by S-nitrosylation has been reported for serine racemase (EC 5.1.1.18, SR), a neuronal pyridoxal 5'-phosphate (PLP)-dependent homodimeric enzyme that catalyzes the reversible racemization of L-serine to D-serine and the irreversible deamination of both L- and D-serine to pyruvate and ammonia [4–15]. D-serine is an obligatory co-agonist of the NMDA glutamatergic receptors and, therefore, the regulation of the activity of SR is crucial to modulate excitatory neurotransmission. SR is expressed in glutamatergic neurons [16], where NO signaling occurs [17]. Early experiments on a human glioblastoma cell line showed that SR was inhibited by NO, an effect reversed by the addition of the substrate [18]. The nitrosylation site of murine SR is Cys113 [19], whereas three nitrosylation sites were found in human SR (hSR): Cys113, Cys269, and Cys218, with the fast modification of Cys113 accounting for almost 70% of inhibition [20]. SR inhibition by S-nitrosylation was suggested as a mechanism to reduce the overstimulation of NMDA neurotransmission, which indirectly activates neuronal NOS (nNOS) and produces cell death. Intriguingly, some known protein interactors of SR are also regulated by S-nitrosylation (PICK1 [21], GAPDH [22]), or colocalize with nNOS (PDS-95 [17]). Glutamatergic receptors NMDA and AMPA are also regulated by S-nitrosylation [23,24].

Besides S-nitrosylation, hSR activity is regulated by ATP and glycine. ATP is a positive allosteric effector of hSR [11] and binds to symmetric sites at the dimer interface, 15 Å away from the active site [25]. Considering a  $K_D^{ATP}$  of around 200 μM [11] and an intracellular concentration in the low millimolar range [26], hSR is predicted to be fully ATP-saturated under physiological conditions. Glycine—an inhibitor of hSR—covalently binds at the active site and is present at intracellular concentrations comparable to its  $K_D$  of 0.47 mM for hSR [27,28], suggesting a partial occupation of SR dimers [29]. L-serine is unlikely to significantly compete, as it exhibits a  $K_M$  of about 12 mM [11]. Direct regulation of SR by glycine is intriguing, considering that (i) D-serine and glycine are co-agonists of NMDA receptors and both act on the same receptor site, (ii) D-serine biosynthesis is linked to that of glycine through the enzyme serine hydroxymethyltransferase, (iii) glycine is a regulator of D-serine release [29], (iv) glycine is a cytoprotectant of several cells, including neurons, in the low

millimolar range, particularly following ATP depletion-associated injury produced by anoxia [30].

From a structural point of view, the binding of ATP, glycine, as well as malonate (MLI), an active-site competitive inhibitor, has been associated with different conformational states of SR. In the absence of active-site ligands or the allosteric effector ATP, *Saccharomyces pombe* SR (SpSR), rat SR, and hSR crystallized in an open conformation, whereas a closed conformation was observed for all homologs when cocrystallized with either the substrate or MLI [25,31–33]. In the closed conformation, the orientation of the two domains forming the hSR protomer changes, with a 20° rotation of the small domain toward the large domain. A third, open-like structure was observed for SpSR cocrystallized with a stable analog of ATP, which produced a change in the relative orientation of the two protomers [25]. Fluorescence spectroscopy of the ATP-hSR complex reveals that this conformation, albeit more similar to the open conformations of SR in the 3D structure, exhibits nevertheless a closer active site in comparison with hSR alone [11].

Herein, we investigated the correlation between S-nitrosylation and the hSR conformations stabilized by ATP and glycine, unveiling a molecular mechanism for hSR regulation by integrating experimental and theoretical approaches.

## Results

### Inhibition of SR by GSNO

Upon incubation with 150 μM GSNO for 5 min in the presence of ATP, the racemase activity of hSR decreased by 66% (Fig. 1A). When glycine was also present in the incubation mixture, the inhibition was only 33% (Fig. 1B). A similar inhibition pattern was observed for the β-elimination activity under the same conditions (Fig. 1C,D). The inhibition of the hSR β-elimination activity brought about by GSNO was also followed kinetically, revealing a biphasic time course with an observed pseudo-first-order rate constant for the fast phase of  $0.59 \pm 0.02 \text{ min}^{-1}$  (Fig. 1E). When glycine was added, the inhibition time course slowed down, proportionally to glycine concentration (Fig. 1E and Table S1). Particularly, in the presence of 3 mM glycine—within its physiological range [28,34]—a 100-fold decrease in the reaction rate with GSNO was observed. The dependence of the reaction rate constants ( $k_{\text{obs}}$ ) on glycine concentration (Fig. 1E, inset), yielded a  $K_{50}^{\text{gly}}$  of  $111 \pm 8 \mu\text{M}$ , indicating that the modulation of S-nitrosylation by glycine takes place at sub-millimolar concentrations. Similar behavior was

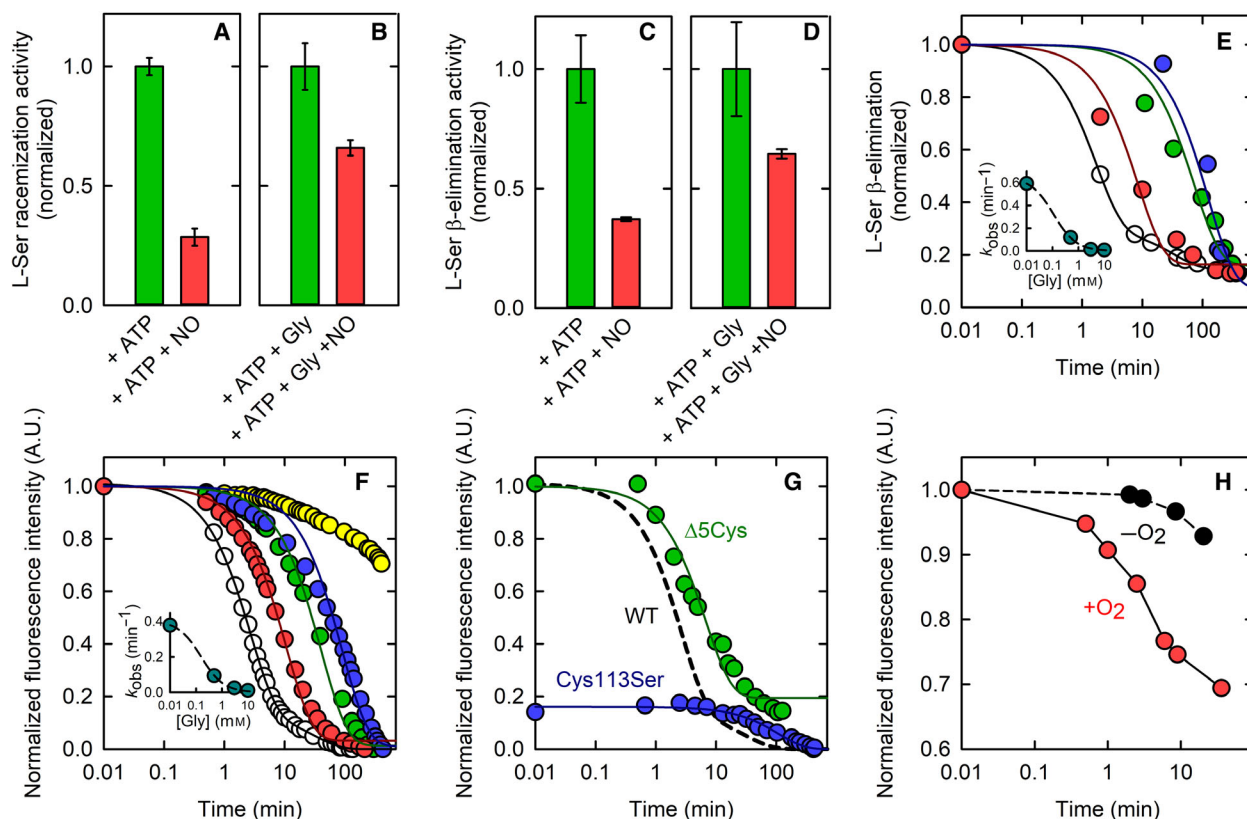


**Fig. 1.** Conformation dependence of WT hSR S-nitrosylation. (A) L-serine (50 mM) racemization by hSR (4 μM) in the presence of ATP (6 mM) before (green bar) and after (red bar) 5-min incubation with GSNO (150 μM); the latter activity was expressed as a fraction of the activity in the absence of GSNO. (B) L-serine racemization under the same conditions as (A) in the presence of 1 mM glycine. (C) L-serine (50 mM) β-elimination by hSR (0.5 μM) in the presence of ATP (6 mM) before (green bar) and after (red bar) 5-min incubation with GSNO (150 μM); the latter activity was expressed as a fraction of the activity in the absence of GSNO. (D) β-Elimination activity under the same conditions as (c) in the presence of 1 mM glycine. The error bars in panels A–D are the S.E.M. of three independent experiments. (E) Initial rate of L-serine (500 mM) β-elimination by hSR (0.4 μM) in the presence of ATP (6 mM) after addition of 150 μM GSNO in the absence (open circles), and presence of 0.5 mM (red circles), 3 mM (green circles), and 10 mM (blue circles) glycine. Enzyme activities at each glycine concentration were normalized to the activity of hSR in the absence of GSNO. Inset: Dependence of the  $k_{\text{obs}}$  resulting from the fitting of the data points of each kinetic trace versus the corresponding concentration of glycine. The dashed line is the fitting of the experimental points to equation 5. (F) Time courses of hSR PLP fluorescence emission upon excitation at 445 nm after the addition of 150 μM GSNO in the absence (open circles) and presence of 0.5 mM (red circles), 3 mM (green circles), 10 mM (blue circles), and 80 mM (yellow circles) glycine. Inset: Dependence of the  $k_{\text{obs}}$  resulting from the fitting of the data points versus the concentration of glycine, the dashed line is the fitting of the experimental points to equation 5. The lines in (E) and (F) are the fitting of the experimental points to equation 2 for hSR in the presence of ATP or equation 3 for hSR in the presence of both ATP and glycine (see text). (G) Time course of fluorescence emission of Cys113Ser hSR (blue) and Δ5Cys hSR (green) in the presence of 6 mM ATP upon addition of 150 μM GSNO. The dashed line is the fitting of the experimental points for WT hSR under the same conditions (Fig. 1F, open circles). The solid lines are the fitting of the experimental points to equation 3 for both Cys113Ser hSR and Δ5Cys hSR. (H) Time course of hSR fluorescence emission after the addition of MAHMA NONOate (95 μM) under a nitrogen atmosphere (closed circles) and in air (red circles)

observed in the presence of MLI (Fig. S1), a competitive inhibitor that stabilizes the closed conformation observed in hSR crystal structures [25,31–33].

### Nitrosylation influences the fluorescence properties of hSR

PLP bound to the active site of hSR emits fluorescence when excited in the visible region, where the internal

aldimine of the cofactor maximally absorbs [11]. An increase in fluorescence emission, accompanied by a blue shift, was observed in the presence of many SR ligands, including ATP and MLI [35], and was attributed to a closure of the active site. L-serine and glycine [11] also produce an increase in fluorescence emission, but the emitting species is the external aldimine of PLP, which exhibits intrinsically different fluorophoric properties with respect to the internal aldimine.

Following incubation of ATP-bound hSR with GSNO, the PLP fluorescence emission spectra upon excitation at 445 nm decreased to values similar to those measured in the absence of ATP (Fig. S2) [20]. Therefore, it was concluded that nitrosylation of hSR stabilizes an open conformation.

The changes in hSR fluorescence induced by the reaction with GSNO were followed kinetically. When GSNO was added to the ATP-bound enzyme, fluorescence emission upon excitation at 445 nm decreased around fourfold in a biphasic process, with an observed rate constant for the fast phase of  $0.380 \pm 0.005 \text{ min}^{-1}$ , consistent with the rate of enzyme inactivation (Fig. 1F). Variant Cys113Ser did not undergo significant changes in fluorescence emission in the same timescale (Fig. 1G). The slower phase observed for both WT and Cys113Ser hSR was previously attributed to the nitrosylation of different cysteine residues [20]. Variant Cys2Ser, Cys4Ser, Cys128Ser, Cys269Ser, Cys309Ser ( $\Delta 5\text{Cys}$ ) hSR exhibited a GSNO-induced S-nitrosylation kinetics only slightly slower than that observed for WT hSR (Fig. 1G), with a pseudo-first-order rate constant of  $0.15 \pm 0.02 \text{ min}^{-1}$ , confirming the association between Cys113 nitrosylation and the observed changes in fluorescence. In this variant, besides Cys113, only Cys46 and Cys217 were retained because they are critical for protein function [19], although they were not observed to be S-nitrosylated [20].

When glycine and ATP were both present in the incubation mixture, the time course of fluorescence emission slowed down proportionally to glycine concentration, similar to what was observed for enzyme activity (Fig. 1F and Table S1). The dependence of the rate constants on glycine concentrations yielded a  $K_{50}^{\text{gly}}$  of about  $159 \pm 12 \mu\text{M}$  (Fig. 1F, inset), closely mirroring the value determined from the enzyme assays (Table S1, Fig. S3). Unlike the latter, fluorescence experiments could be carried out at high concentrations of glycine, as the detection did not depend on the residual activity of the enzyme. At 80 mM glycine—170-fold the  $K_D$  [11]—only a slow phase was observed (Fig. 1F). All fluorescence and enzyme activity changes were reverted by the addition of the reducing agent TCEP (data not shown).

Inside cells, cysteine nitrosylation can either result from transnitrosylation by nitroso donors or from a direct, oxygen-dependent reaction of the cysteine residue with NO. Therefore, we checked the reactivity of hSR with the diazeniumdiolate quick-releasing NO donor MAHMA NONOate, which dissociates into NO in aqueous solutions within minutes. In the presence of  $95 \mu\text{M}$  NO, fluorescence emission decreased

over time (Fig. 1H) similarly to what was observed in the presence of GSNO at comparable concentrations. When the reaction was carried out under anaerobic conditions, the reaction rate decreased approximately 10-fold, confirming an oxygen-dependent S-nitrosylation mechanism.

### S-nitrosylation detection by differential tagging

As both enzyme assays and fluorescence experiments suggested the dependence of S-nitrosylation on the binding state of hSR, we pursued a differential tagging strategy that we named 5-IAF switch method and which allows for the tagging of nitrosylated cysteine side chains with a fluorescein-based tag (see Materials and Methods). The protocol was applied to hSR in different ligation states, known to correspond to different conformations, as inferred from the crystal structures of SpSR, rat SR, and hSR [25,31–33]. The results of the 5-IAF switch method are reported in Fig. 2A. In the presence of only  $\text{Mg}^{2+}$ , which binds at a specific site in the large domain and activates the enzyme 10-fold [25,33,36–38], a faint fluorescence band was observed, indicating that the protein was poorly nitrosylated by GSNO. Under these conditions, SR is known to assume an open conformation from the crystallographic structure of all orthologues [25,31–33]. In the presence of EDTA, which chelates  $\text{Mg}^{2+}$  and completely inactivates the enzyme [36], a similarly faint band was detected (Fig. 2A). No crystal structure under these conditions is available, but spectroscopic experiments suggested an open-like conformation [36]. In the presence of 6 mM ATP and  $\text{Mg}^{2+}$ , the fluorescent band in the gel was threefold more intense than in the presence of  $\text{Mg}^{2+}$  alone, suggesting that the conformation stabilized by ATP is significantly more prone to nitrosylation. When glycine was also added, a less intense band was observed, whereas an intermediate behavior was observed when both ATP and glycine were present (Fig. 2A).

The quantitative analysis of Cys113 nitrosylation levels in the presence of different ligands was carried out by mass spectrometry of the trypsin digests of the 5-IAF-modified proteins (Fig. 2B). The peptide LEGIPAYIVVPQTAPDCK, containing Cys113, was identified in all samples upon tryptic digestion of hSR, either originally nitrosylated (in which cysteine is modified with 5-IAF) or unmodified (in which cysteine is modified with IAA), depending on the conditions (Table 1). In the presence of ATP alone and in the presence of both ATP and glycine, a higher MS/MS coverage was observed in comparison with the other conditions (Table S2). The relative AUCs of the

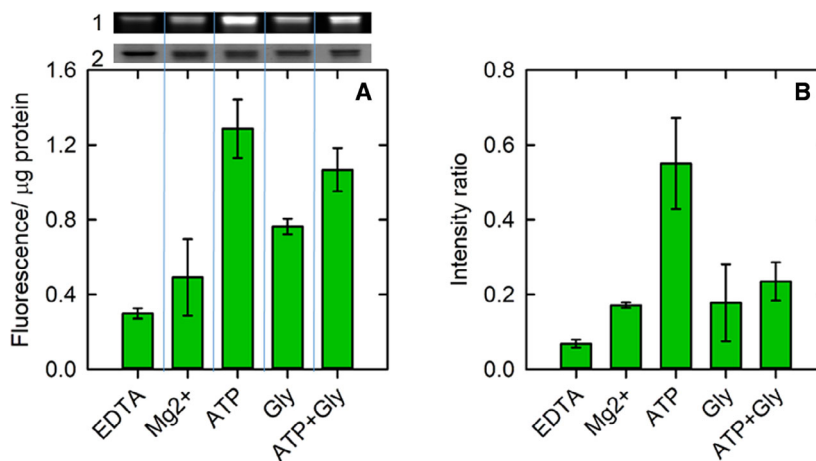


**Fig. 2.** Quantification of nitrosylation levels of SR. (A) 5-IAF switch method applied to hSR incubated with 150 μM GSNO for 90 min in the presence of: 5 mM EDTA (EDTA); 10 mM MgCl<sub>2</sub> (Mg<sup>2+</sup>); 6 mM ATP and 10 mM MgCl<sub>2</sub> (ATP); 80 mM glycine and 10 mM MgCl<sub>2</sub> (Gly); 6 mM ATP, 10 mM MgCl<sub>2</sub> and 80 mM glycine (ATP + Gly). For each condition, 0.5 μg of GSNO-incubated hSR was run in SDS/PAGE; the fluorescence emitted by the hSR bands (panel 1) and their Coomassie blue staining intensity (panel 2) was measured. The bars are the ratios between the two signals (in arbitrary units) for each condition. The error bars are the S.E.M. of three independent experiments. (B) Analysis of liquid chromatography–mass spectrometry experiments on the tryptic digests of the samples of panel (A). The bars are the AUCs of the chromatographic peak of the 5-IAF-modified peptide LEGIPAYIVPQTAPDCK divided by the sum of the AUCs of both 5-IAF-modified and IAA-modified peptides for the same conditions described in (A) (see text). The error bars are the S.E.M. of three independent experiments

chromatographic peaks of the two peptides indicated that the yield of nitrosylation of Cys113 in the presence of only ATP was three times higher than in the presence of both ATP and glycine (Fig. 2B).

### Molecular dynamics simulations of hSR

To understand the molecular bases of the inhibition by S-nitrosylation and the effect of glycine, we performed molecular dynamics (MD) simulations on four ATP-

bound hSR forms: the internal aldimine state (hSR<sup>MD</sup>); the internal aldimine state with nitrosylated Cys113 (NOhSR<sup>MD</sup>); the external aldimine state with glycine (hSR-Gly<sup>MD</sup>); the external aldimine state with glycine and nitrosylated Cys113 (NOhSR-Gly<sup>MD</sup>) (Fig. 3, see Materials and Methods for a more detailed description of the models). All models were submitted to 1 μs-long plain MD simulation.

The RMSD along the trajectories of the homodimer and of the single protomers—hereafter indicated

**Table 1.** Retention time (R.T.), m/z, and observed modification (MOD.) for the modified tryptic peptide LEGIPAYIVPQTAPDCK under all investigated conditions (see text)

	Peptide					
	LEGIPAYIVPQTAPDC(+387.07)K			LEGIPAYIVPQTAPDC(+57.02)K		
	m/z	R.T. (min)	MOD.	m/z	R.T. (min)	MOD.
hSR + EDTA	767.6970 (z = 3)	36.25	5-IAF	986.0158 (z = 2)	31.27	IAA
hSR + Mg <sup>2+</sup>	767.6962 (z = 3)	36.29	5-IAF	986.0148 (z = 2)	31.33	IAA
hSR + ATP	767.6965 (z = 3)	36.16	5-IAF	986.0151 (z = 2)	31.14	IAA
hSR + Gly	767.6970 (z = 3)	36.34	5-IAF	986.0165 (z = 2)	31.32	IAA
hSR + ATP + Gly	767.6978 (z = 3)	36.27	5-IAF	986.0159 (z = 2)	31.25	IAA



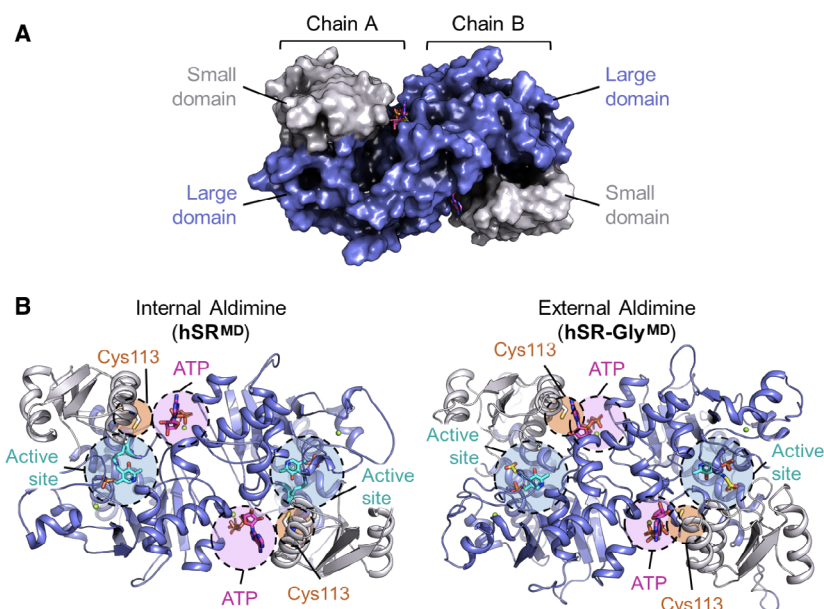


**Fig. 3.** Model of human serine racemase. (A) Surface representation. The small and large domains are colored in gray and lilac, respectively. ATP is shown in capped sticks. (B) Cartoon-like representation of the internal and external aldimine states. ATP, PLP, and Cys113 are labeled and shown in capped sticks. All the images were prepared with PyMOL version 2.3.4

as chains A and B, according to PDB [1wtc](#)—is reported in Table S3 and Fig S4. The RMSD is relatively high, possibly because the models were obtained by homology modeling. The  $\text{hSR}^{\text{MD}}$  and  $\text{hSR-Gly}^{\text{MD}}$  models, corresponding to the complexes with ATP and ATP + glycine, respectively, are quite stable. On the contrary, the corresponding nitrosylated forms ( $\text{NOhSR}^{\text{MD}}$  and  $\text{NOhSR-Gly}^{\text{MD}}$ ) exhibit higher RMSD values, indicating a gradual and consistent conformational distancing from the starting model.

This hypothesis was confirmed by essential dynamics (ED), carried out to uncover the principal modes that describe the overall dynamics. The corresponding principal component analysis (PCA) plots (first vs second component) are shown in Fig. S5 and report the relevant conformational transitions in the near-constraint subspace. The PCA of  $\text{hSR}^{\text{MD}}$  and  $\text{hSR-Gly}^{\text{MD}}$  showed the least variance and converge around half of the simulation. On the contrary, the nitrosylated systems  $\text{NOhSR}^{\text{MD}}$  and, in particular,  $\text{NOhSR-Gly}^{\text{MD}}$  showed a more dispersed PCA plot.

The radius of gyration  $R_g$  was also calculated to describe the compactness of the structure along the trajectory (Table S4 and Fig. S6).  $\text{hSR}^{\text{MD}}$  and  $\text{NOhSR}^{\text{MD}}$  followed the same trend, with an almost identical average  $R_g$ . In  $\text{hSR-Gly}^{\text{MD}}$ ,  $R_g$  decreased over the simulation time, implying a progressively more stable and more compact structure. On the contrary,  $\text{NOhSR-Gly}^{\text{MD}}$  recorded the highest  $R_g$  values, with a rough curve indicating disturbance in the compactness of the structure. The results pointed to an unreliable conformation consistently with the

experimental data indicating that the concomitant presence of glycine and nitrosylated Cys113 is unfavored.

To assess further the effect of glycine and Cys113 nitrosylation on the overall protein flexibility, the root-mean-square fluctuation (RMSF) of each residue around its average position was calculated for each chain of the homodimer (Fig 4). Areas with high fluctuations mainly include the small domain (residues 78–155, peaks 3, 4, and 5 in Fig 4, Panel 1), and the H13–H14 loop in the large domain (peak 6 in Fig. 4, Panel 1). Seemingly, chain A is more flexible than chain B. The nitrosylation increased the flexibility, in particular in  $\text{NOhSR-Gly}^{\text{MD}}$ , which shows the highest RMSF peaks. On the contrary, the lowest RMSF curve belongs to  $\text{hSR-Gly}^{\text{MD}}$ , as the binding of glycine decreases the degrees of freedom, particularly in the loop between helices H13 and H14 (for the location of secondary structure elements in human SR, see Fig. S7).

To assess the variety of conformational populations produced by MD, we performed a clustering with the k-means algorithm (Table S5, Fig. S8). From the most populated cluster, a medoid was extracted and taken as the structure representing the outcome of the MD simulations for each configuration. The extracted medoids were superimposed to the last step of the equilibration before starting the MD production, and vectors were drawn to highlight the directions of the displacement (Fig. 5). We noted that, unlike in  $\text{hSR}^{\text{MD}}$  and  $\text{hSR-Gly}^{\text{MD}}$  (Fig. 5A,C), in the nitrosylated systems  $\text{NOhSR}^{\text{MD}}$  and  $\text{NOhSR-Gly}^{\text{MD}}$  (Fig. 5B,D), the small domain shifted away from the dimer interface,

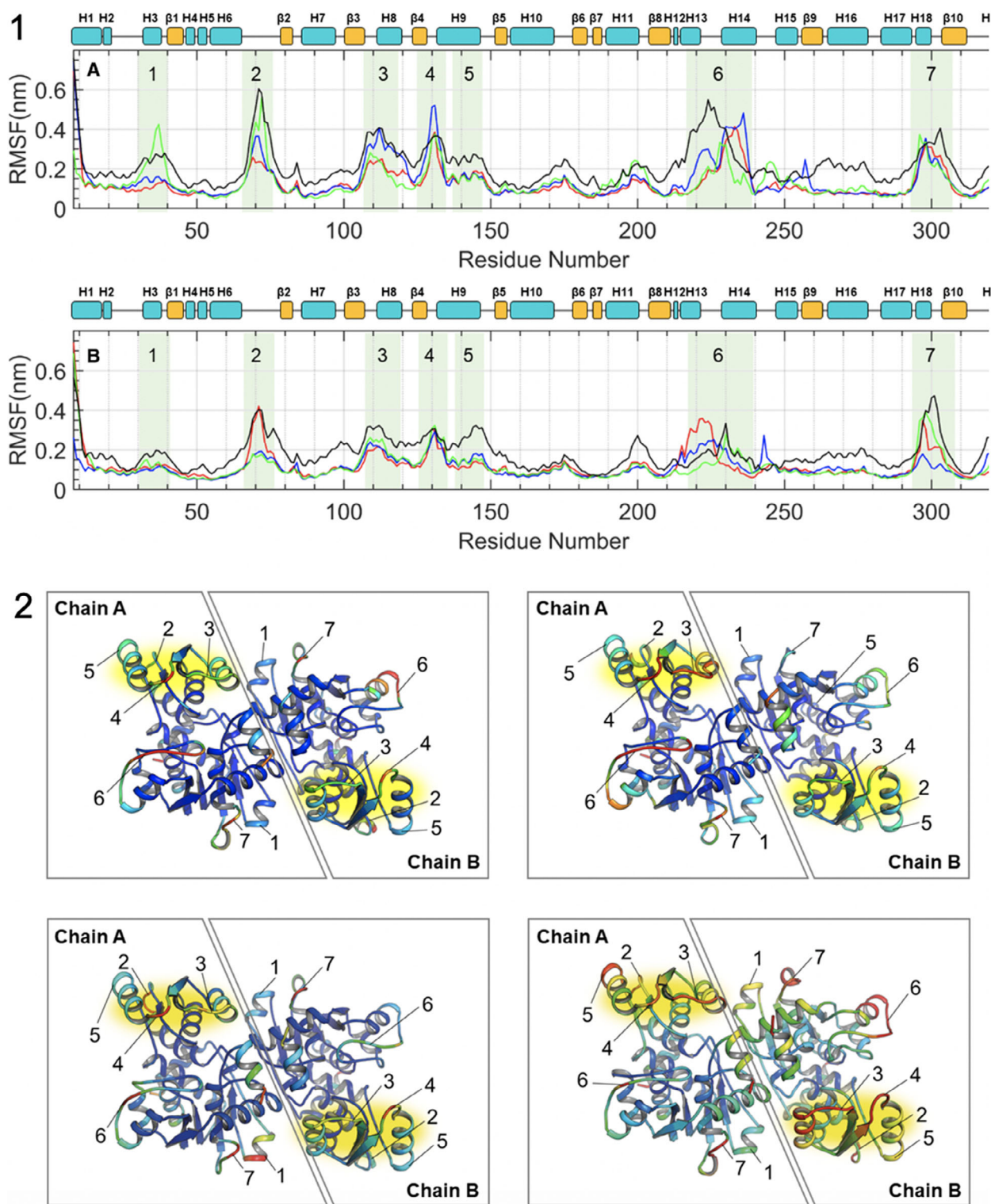


**Fig. 4.** Panel 1. Comparison of the C $\alpha$  atoms RMSF (nm) calculated for the four configurations: hSR<sup>MD</sup> (red), NOhSR<sup>MD</sup> (blue), hSR-Gly<sup>MD</sup> (green), NOhSR-Gly<sup>MD</sup> (black). (A) Chain A. (B) Chain B. Light green bands highlight regions of the polypeptide chain with RMSF peaks. The numbers refer to the 3D structure (see Panel 2). The small domain includes the regions 3, 4, and 5. Panel 2. RMSF color-code representation. a. hSR<sup>MD</sup>. b. NOhSR<sup>MD</sup>. c. hSR-Gly<sup>MD</sup>. d. NOhSR-Gly<sup>MD</sup>. Colors range from cold shades (blue, low RMSF) to warm shades (red, high RMSF). Protomers have been indicated in each panel. Small domains have been highlighted with a yellow background. Numbers correspond to the numbered peaks in Panel 1. The structures of Panel 2 were generated with Pymol 2.4.1

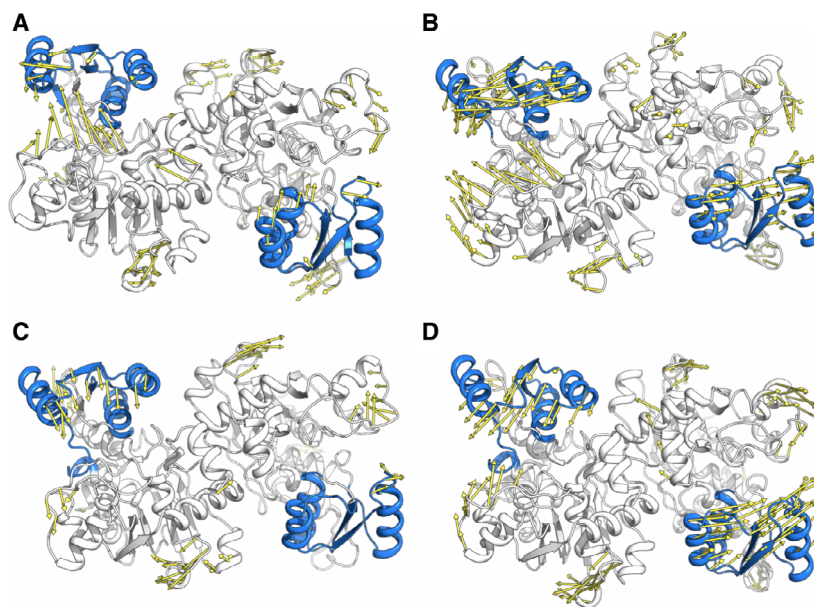


**Fig. 5.** Vectors (yellow arrows) showing the displacement between the last equilibration step (shown as cartoon) and the medoid for each trajectory. a.  $\text{hSR}^{\text{MD}}$ . b.  $\text{NOhSR}^{\text{MD}}$ . c.  $\text{hSR-Gly}^{\text{MD}}$ . d.  $\text{NOhSR-Gly}^{\text{MD}}$ . The yellow arrows indicate the direction and the magnitude of the dynamic transition that occurred during MD simulations. The small and large domains are colored blue and white, respectively. Ligands and ions are omitted for clarity

with a quasi-rigid body motion. This concerted movement allowed the nitrosylated side chain of Cys113 to find its way to the solvent, avoiding the steric hindrance and electrostatic repulsion of surrounding residues.

The higher flexibility of the small domain in the nitrosylated systems was also highlighted by the DynDom software [39], which detects rigid body interdomain rotations and closure motions. Considering the small domain as flexible and the large one as fixed, large angles of rotations were determined for  $\text{NOhSR}^{\text{MD}}$  and  $\text{NOhSR-Gly}^{\text{MD}}$ , while medium-to-low angles of rotations were registered for  $\text{hSR}^{\text{MD}}$  and  $\text{hSR-Gly}^{\text{MD}}$ . The corresponding degree of closure is reported in Table S6. In  $\text{hSR}^{\text{MD}}$ , chain A showed a clear motion, which was not detected in chain B (83% and 9% for chains A and B, respectively), again supporting the different behavior of the protomers. As expected,  $\text{hSR-Gly}^{\text{MD}}$  showed the highest degree of closure (94% and 78% for chains A and B, respectively), reflecting the decrease in radius of gyration along the trajectory. On the contrary, a lower degree of closure was associated with the small domain movement in the nitrosylated configurations  $\text{NOhSR}^{\text{MD}}$  (41% and 28%) and  $\text{NOhSR-Gly}^{\text{MD}}$  (59% and 33%). The latter showed unclear behavior, with the two chains acting differently. This dynamic asymmetry is likely the result of a large unbalance of the system, in which two opposite forces are acting: Cys113 nitrosylation, which tends to push the small domain away from the large one, and glycine binding, which draws the small and the large domains closer. This effect is

mirrored by the changes in fluorescence emission, which decreased upon nitrosylation and increased in the presence of ATP, glycine, or MLI (Fig. S2) suggesting an opening and a closing of the active site, respectively.

We also evaluated the occupancy of the hydrogen bonds formed by ATP with the surrounding residues, as well as the electrostatic contacts formed at the dimer interface in the different configurations (data not shown). No significant effect or variation was observed upon nitrosylation. According to these observations, we hypothesize that the NO-mediated inhibition of the enzyme activity is allosterically driven by the detachment of the two domains and, consequently, by the impossibility for the enzyme to stabilize the active conformation, rather than by a direct effect on ATP binding.

### Mechanism of hSR inhibition by S-nitrosylation

To evaluate how the relative motion of the small and large domains modulated by Cys113 nitrosylation affects enzyme activity, we compared the crystallographic structures of SR in the open and closed forms in the surroundings of the catalytic residue Ser84 [25,31–33]. The opening of the small domain moves Ser84 away from the substrate, thus preventing catalysis (Fig. 6). We speculate that, as long as Cys113 remains nitrosylated, the small domain cannot close on the large one because of the electrostatic and steric hindrance between the nitroso group of Cys113 and the surrounding residues, particularly Asp318. We



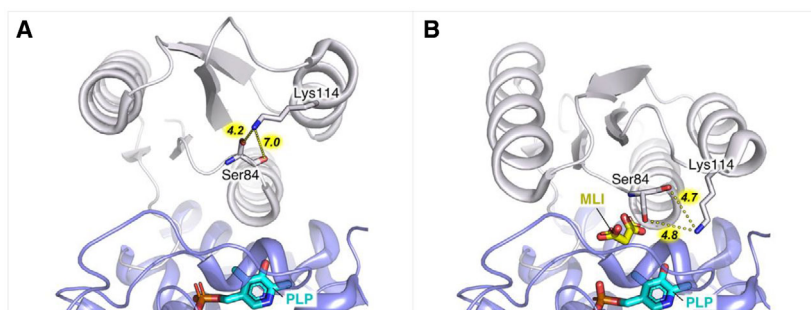


**Fig. 6.** Role of Lys114. (A) Open form of hSR (PDB code 5X2I). (B) Closed form (PDB code 316B). The protein is shown as cartoon. ATP, Ser84, Lys114, PLP, and MLI are labeled and shown as capped sticks. The distance between the catalytic Ser84 and Lys114 is labeled and displayed as yellow dashed lines

further explored this assumption by focusing on Lys114. In the open or open-like X-ray structures (PDB codes 1V71, 5X2I, 1WTC), Lys114 stabilizes Ser84 with a hydrogen bond, keeping it away from the catalytic site (Fig. 6A). When a substrate or an inhibitor is bound (PDB codes 3I6B, 3I6R, 3I6C, 2ZPU, 2ZR8), the loop between  $\beta$ 2 and helix H7 (residues 83–84–85) behaves as a nest motif, coordinating the carboxylate of the substrate. During this loop reorganization, Ser84 is pulled down to the active site, allowing catalysis (Fig. 6B), while the small domain closes on the large one. Once the product of the catalysis is released, residues 84–85 should unfold back to a disordered loop, and the small domain recovers its flexibility, resulting in an overall open conformation. Therefore, the activity of the enzyme depends on its ability to reach a fully closed conformation stabilized by the simultaneous binding of active-site ligands (L-serine, D-serine, MLI, or glycine) and ATP (Fig. S9). The nitrosylation of Cys113, acting as a wedge, prevents the attainment of the closed conformation, thus impairing the catalytic activity.

### Structural determinants of Cys113 S-nitrosylation

In the search for the structural determinants responsible for the reactivity of Cys113 in the different conformations of hSR, we inspected the available crystallographic structures of SRs and our MD simulations (Fig. 7A,B). Cys113 is on the N terminus of helix H8, in the small domain. The closest neighboring residues are on the same helix H8 (Lys114), on the large domain in the loop between the  $\beta$ -strand  $\beta$ 10 and helix H19 (Asn316 and Asp318), and on the symmetric subunit (Glu276). The distance between these residues and Cys113 changes significantly depending on the ligation state of SR. Particularly, in hSR-Gly<sup>MD</sup>, the presence of a ligand at the active site induces the closure of the small domain and increases the proximity of Cys113 to Asp318 (Fig. 7B) [25,31–33]. Interestingly, multiple sequence analysis SR orthologues indicated high

conservation for the residues that are in close proximity to Cys113 (Fig. 7C).

To identify further residues that might affect Cys113 nitrosylation and mediate the allosteric communication between the active site and the ATP binding site, we carried out a network analysis on hSR<sup>MD</sup>, NOhSR<sup>MD</sup>, hSR-Gly<sup>MD</sup>, and NOhSR-Gly<sup>MD</sup> medoids. In Fig. S10, we reported the network of contacts built around Cys113, ATP, and PLP in chain A (panels a, c, e, g) and chain B (panels b, d, f, h). In hSR<sup>MD</sup> and NOhSR<sup>MD</sup>, a hydrogen bond network connecting ATP to PLP through Asn316, Glu283, Asn86 was detected only in one chain of the dimer (panels b and c), suggesting structural asymmetry when no ligand is bound at the active site. Contrarily, in hSR-Gly<sup>MD</sup> (panels e and f), glycine stabilizes the polar path involving Asn316, Glu283, Asn86 in both chains A and B. However, this symmetry cannot be detected in NOhSR-Gly<sup>MD</sup>, in which the effect of nitrosylation overruled that of glycine, resulting in a uniquely disrupted residue network pattern not found in any other trajectory (panel h). The residue interaction network analysis brought to light the fundamental role of Asn316 as the polar bridge between ATP and the PLP clusters. The residue network analysis also showed, in one of the two chains of hSR<sup>MD</sup> and hSR-Gly<sup>MD</sup>, a generic contact between Cys113 and Asp318. Despite the proximity of the side chains of both amino acids, no relevant polar contact between Asp318 and Cys113 was found throughout MD simulations (data not shown).

### Characterization of hSR variants

To explore the hints provided by MD simulations, we designed, expressed, and characterized hSR variants Lys114Gln, Asn316Ala, Asp318Ala, Asp318Asn, and Glu276Gln (Table 2). The characterization of hSR variants Asp318Asn, Gln89Met, and Cys113Ser has already been reported [20,40]. The residues we mutated included those neighboring Cys113 (Fig. 7B): Gln89,

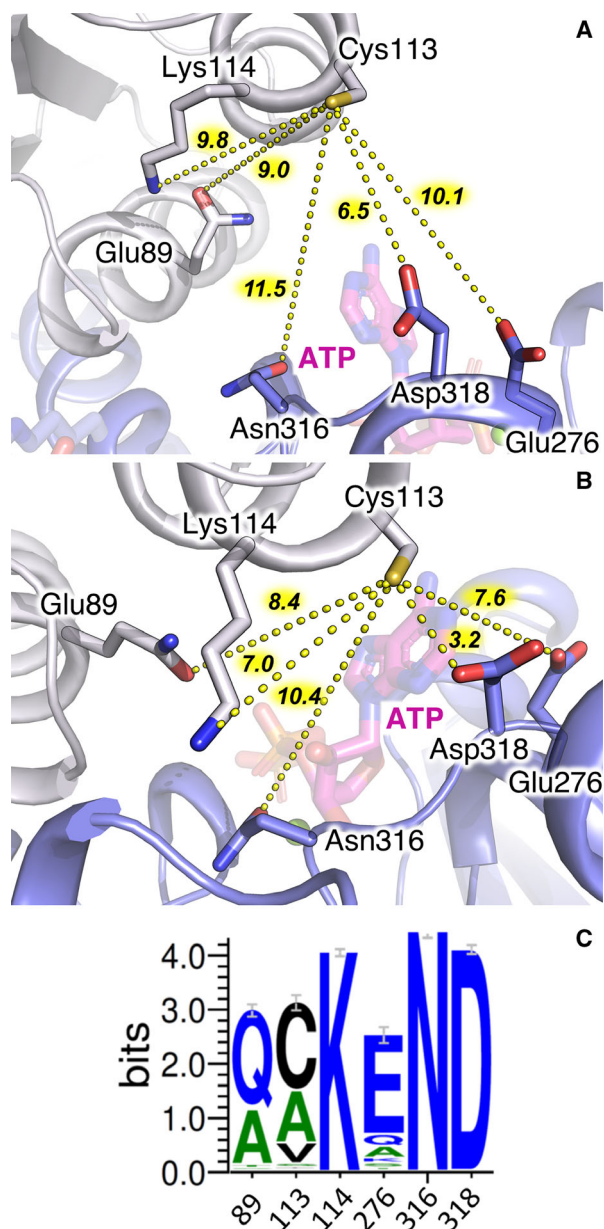


**Fig. 7.** Cys113 surroundings and residue conservation in hSR<sup>MD</sup> (A) and hSR-Gly<sup>MD</sup> (B). The protein is shown as cartoon. Cys113 and the surrounding residues are labeled and shown as capped sticks. ATP is labeled and shown as transparent ball and sticks for clarity. The distances among the residue side chains are labeled and displayed as yellow dashed lines. (C) Logo plot of the alignment of Cys113 and spatially neighboring amino acids. The analyzed sequences were from 9800 serine racemase orthologues

whose importance was discussed in our previous work [40]; Asn316, Lys114, Asp318, whose role was suggested by our MD simulations (see above); Glu276 of the symmetric unit, for its proximity to Cys113 in hSR

X-ray structures. The kinetic parameters of all the variants are reported in Table 2.

Variants Asp318Ala and Asp318Asn were fully active, with a twofold and threefold higher  $K_M$  in comparison with WT hSR for the  $\beta$ -elimination of L-serine, respectively, and a lower  $k_{cat}$ . They both bound ATP cooperatively with a 2-/3-fold lower affinity compared to WT hSR. It is interesting to note that Asp318 is invariant in all SRs within the conserved sequence GGNVDL (Fig. 7C), including the forms not exhibiting a cysteine residue at position 113.

Variant Asn316Ala exhibited a  $k_{cat}$  22-fold lower than WT hSR and a threefold higher  $K_M$  for L-serine. It was not activated by the presence of ATP (data not shown) and it did not undergo any changes in fluorescence emission upon ATP addition (Fig. S11). Consistently, no fluorescence emission decay was observed in the presence of ATP upon incubation with GSNO (Fig. 8C). These findings confirmed the prediction of the residue interaction network analysis (Fig. S10), which suggested that any mutation of this residue disrupting the hydrogen bond network interrupts the allosteric communication between the ATP and PLP sites. It should be noticed that Asn316 is involved in a hydrogen bond with the ribose group of ATP according to the crystal model of SpSR [25] and its mutation is therefore likely to prevent ATP binding.

As Asp318, Lys114 is invariant in all SRs (Fig. 7C). The Lys114Gln variant exhibited a  $K_M$  close to that of WT hSR, but a 26-fold lower  $k_{cat}$ . The  $K_D$  for ATP was only slightly lower than that of WT hSR, but its binding did not show any cooperativity. It was inferred that Lys114 is crucial in activating Ser84 by lowering its  $pK_a$  [41], thus explaining the low observed  $k_{cat}$ . The lack of cooperativity in ATP binding suggested that this conserved residue is also relevant in the allosteric communication between the active site and the ATP binding site.

The mutation of Glu276 to glutamine increased the  $K_M$  for L-serine twofold, but the  $k_{cat}$  remained close to that of WT hSR. This variant bound ATP with minimal cooperativity but with a  $K_D$  similar to that of WT hSR.

### Reactivity of hSR variants with GSNO

For all variants, the inhibition produced by 150  $\mu$ M GSNO was evaluated in the presence of either ATP (Fig. 8A) or both ATP and glycine (Fig. 8B). The same experiment was also carried out for WT hSR in the presence of the triphosphonucleotides GTP and CTP to assess the effect of the nucleobase, the moiety of the nucleotide closer to Cys113. The time courses of

**Table 2.** Kinetic parameters ( $\beta$ -elimination) and ATP binding parameters for variants used in this study. Enzyme assays were performed at 37 °C. ATP activation is the ratio between the  $V_{\max}$  at 6 mM ATP and in the absence of ATP. The values of  $K_M$  and  $k_{\text{cat}}$  for L-serine  $\beta$ -elimination were obtained fitting the data points with equation 1, while for ATP binding parameters, equation 4 was used. For variant Asn316Ala, which does not bind ATP, the ATP binding parameters are not reported

Variant	$K_M$ , L-serine (mM)	$k_{\text{cat}}$ ( $\text{min}^{-1}$ )	$k_{\text{cat}}/K_M$ ( $\text{min}^{-1}\text{mM}^{-1}$ )	$K_D$ ATP (mM)	nATP	ATP activation	Ref.
WT hSR	16 ± 1	166 ± 10	10.4	0.21 ± 0.01	1.8 ± 0.2	10	[20]
Cys113Ser	54 ± 5	51 ± 2	0.9	1.07 ± 0.06	1.6 ± 0.2	9.5	[20]
Cys2Ser, Cys4Ser, Cys128Ser, Cys269Ser, Cys309Ser ( $\Delta 5\text{Cys}$ )	48 ± 9	57 ± 3	1.2	0.24 ± 0.05	1.7 ± 0.5	10	This work
Asp318Asn	50 ± 3	115 ± 2	2.3	0.68 ± 0.03	1.8 ± 0.1	9.5	[20]
Asp318Ala	33 ± 6	70 ± 3	2.1	0.52 ± 0.05	1.6 ± 0.2	7.5	This work
Asn316Ala	41 ± 1	7.6 ± 0.1	0.2	-	-	-	This work
Lys114Gln	19 ± 1	6.3 ± 0.1	0.3	0.11 ± 0.04	0.8 ± 0.2	2.1	This work
Gln89Met	19 ± 2	56 ± 1	2.9	0.15 ± 0.01	1	3.9	[40]
Glu276Gln	34 ± 5	133 ± 6	3.9	0.28 ± 0.03	1.5 ± 0.4	7.8	This work

fluorescence emission upon incubation with GSNO were also followed, either in the presence of ATP (Fig. 8A and Fig. S12a) or ATP and glycine (Fig. 8B and Fig. S12b).

In the presence of ATP, all variants showed a significant decrease in activity upon a 5-minute incubation with GSNO, except for Cys113Ser—which lacks the reactive cysteine—and Lys114Gln, which showed minimal inhibition (Fig. 8A). The lower degree of inactivation was reflected in a slower time course of the decrease in fluorescence emission for variant Lys114Gln, with a rate constant of  $0.069 \pm 0.002\text{min}^{-1}$ , and a fractional decay after 5 min comparable to the decrease in activity (Fig. 8C and Fig. 8A). Lys114 was therefore confirmed as the basic residue responsible for the activation of Cys113 toward nitrosylation. In the presence of ATP only, variants Glu276Gln, Asp318Ala, and Asp318Asn exhibited behavior similar to that of WT hSR for both enzyme assay and fluorescence measurements (Fig. 8A,C, Fig. S13), ruling out that either Glu276 or Asp318, despite their relative closeness to Cys113 (Fig. 7), modulates its nitrosylation in the conformation stabilized by ATP. Particularly, in ATP-bound forms, Asp318 is ruled out as the acidic residue of a putative acid–base dyad, as it was proposed [19].

Activity inhibition by S-nitrosylation took place also when ATP was substituted by CTP or GTP (Fig. 8A). The adenosine group is the closest to Cys113 (Fig. 7) and was suggested to be responsible for the activation of Cys113 [19]. However, the ATP binding site is poorly selective in terms of nucleobase, but it requires a triphosphate ribose moiety [5]. Indeed, when adenine was substituted by guanine and even by the pyrimidine cytosine, S-nitrosylation took place, suggesting an

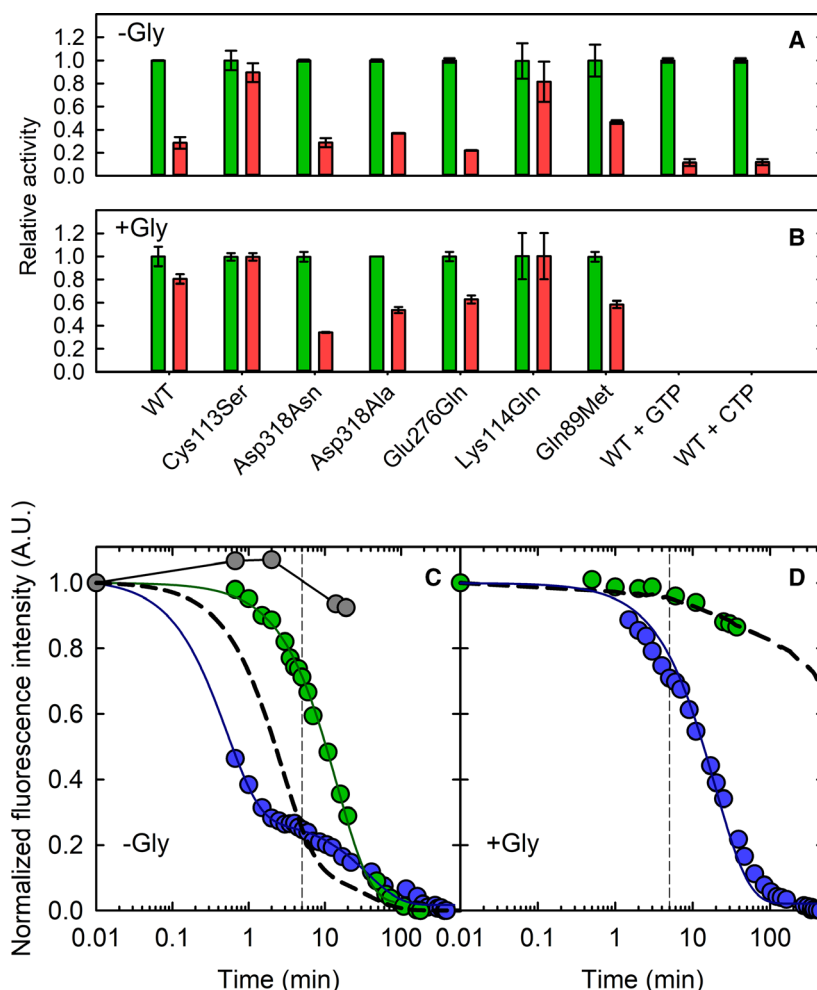
allosteric effect of the nucleotide on S-nitrosylation, rather than a direct interaction between Cys113 and the nucleobase.

When 6 mM glycine was added to the reaction mixture, the degree of inactivation in 5 min was lower for hSR and its variants (Fig. 8B), with the notable exception of Asp318Ala and Asp318Asn, which were inhibited to the same extent in the presence and absence of glycine. Consistently, the nitrosylation kinetics monitored by fluorescence showed that variants Asp318Asn and Asp318Ala were only modestly slowed down in the presence of ATP and a high concentration of glycine (i.e. 80 mM, approximately 170-fold the  $K_D$ ) (Fig. 8D, Fig. S13), with a pseudo-first-order constant of  $0.052 \pm 0.003\text{min}^{-1}$  and  $0.089 \pm 0.004\text{min}^{-1}$ , respectively. This result pointed to Asp318 as the residue responsible for the loss of Cys113 reactivity in the conformation stabilized by ATP and glycine. Variant Glu276Gln exhibited a slightly higher degree of GSNO-induced inhibition both in the presence of ATP and in the presence of ATP and glycine. The Gln89Met variant exhibited a similar behavior in both conditions, suggesting that this variant is less sensitive to the effect produced by ATP and glycine, possibly due to disrupted communication between the ATP binding site and the active site, as observed previously [40] (Fig. 8A,B).

### Evaluation of the role of Lys114 and Asp318 in conformation-dependent Cys113 reactivity

As Lys114 and Asp318 were identified as the residues affecting Cys113 nitrosylation, we focused on their behavior in our MD simulations and on their effect on the  $pK_a$  of Cys113.

**Fig. 8.** S-nitrosylation of hSR variants. (A)  $\beta$ -Elimination of L-serine (500 mM) by ATP-bound WT hSR and its variants (0.5  $\mu$ M) pre-incubated for 5 min in the presence (red bars) or absence (green bars) of 150  $\mu$ M GSNO. (B)  $\beta$ -Elimination of L-serine by hSR and its variants in the same conditions as (A) with the additional presence of 6 mM glycine. The activities are reported as a fraction of the activity measured in the absence of GSNO for each variant. The assays for hSR incubated with nucleotides GTP and CTP instead of ATP are also reported. (C) Time course of fluorescence emission for Asp318Asn hSR (blue circles), Lys114Gln hSR (green circles), and Asn316Ala hSR (gray circles) upon addition of 150  $\mu$ M GSNO in the presence of 6 mM ATP. (D) Time course of fluorescence emission for Asp318Asn hSR (blue circles) and Lys114Gln hSR (green circles) upon addition of 150  $\mu$ M GSNO in the presence of 6 mM ATP and 80 mM glycine. The black dashed lines are the corresponding kinetics reported for WT hSR in Fig. 1. Except for Asn316Ala variant, the solid lines are the fitting of the experimental points either with equation 2 for Asp318Asn in the presence of ATP or equation 3 for Lys114Gln in the presence of ATP or Asp318Asn in the presence of ATP plus glycine. All error bars are the S.E.M. of three independent experiments



We first measured the distance between Cys113 and Lys114 in the hSR<sup>MD</sup> and hSR-Gly<sup>MD</sup> non-nitrosylated systems. In the open chain A of hSR<sup>MD</sup> (panel a in Fig. S14), the baseline of the distance between the side chains of Cys113 and Lys114 was quite stable (~ 3.2 Å), but possibly underestimated, since MD cannot deal with the thiol-thiolate equilibrium and, therefore, the interaction between Lys114 and the thiolate form of Cys113 could not be evaluated. The PROPKA 3.0-estimated pK<sub>a</sub> [42] of Cys113 in the hSR<sup>MD</sup> medoid was 9.08, approximately the same as for free cysteines. However, in frames where the Lys114-Cys113 distance was short and Cys113 buriedness low, Cys113 pK<sub>a</sub> was assessed to be around 8.70, indicating that Lys114 can stabilize the thiolate form of Cys113 and activate it toward nitrosylation, in agreement with the experimental results on the Lys114 variants. During the transition to a closed form in the hSR-Gly<sup>MD</sup> system (panels c, d in Fig. S14), the distance between Cys113 and Lys114 was higher than in the hSR<sup>MD</sup>

system, consistently with a lower reactivity of Cys113 in the glycine-bound form, as experimentally observed. Finally, in the NOhSR<sup>MD</sup> trajectories, the distance between Lys114 and nitrosylated Cys113 was around 3 Å (Fig. S15), supporting an additional role of Lys114 in stabilizing the nitrosylated Cys113.

We then focused on the acidic residue Asp318 and measured its distance from Cys113 in the non-nitrosylated systems hSR<sup>MD</sup> and hSR-Gly<sup>MD</sup> (Fig. S16). In hSR<sup>MD</sup>, the side chain of Cys113 moved away from the carboxyl group of Asp318 in chain A due to the opening of the protomer. On the other hand, in chain B, the distance between Cys113 and Asp318 decreased, while the protomer closed. In hSR-Gly<sup>MD</sup>, oscillations in the distance seemed to exclude a persistent hydrogen bond between the two, suggesting that Asp318 may have a role in modulating Cys113 pK<sub>a</sub> by affecting the local electrostatic strength, rather than by establishing a direct hydrogen bond. Cys113 pK<sub>a</sub> in the hSR-Gly<sup>MD</sup> medoid was estimated to be 11.11, two-and-a-half units



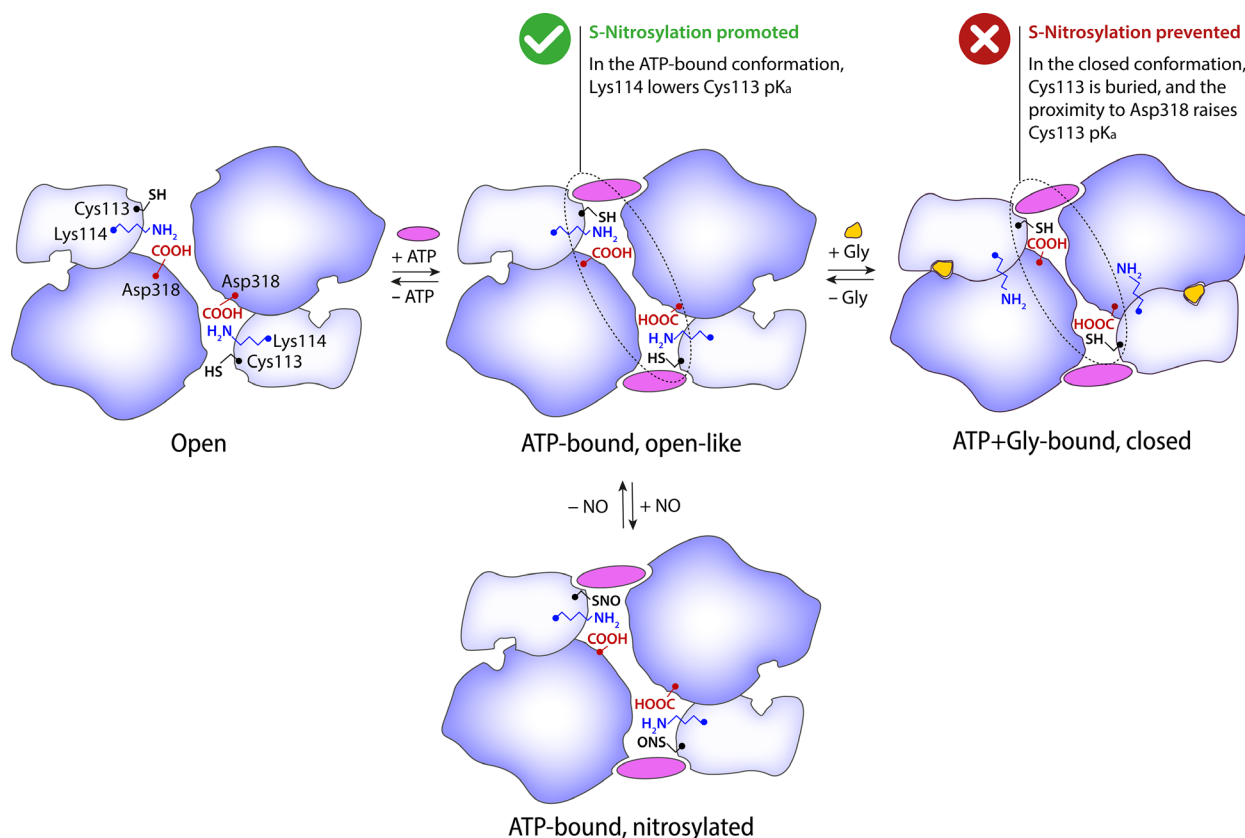


**Fig. 9.** Proposed model of conformation-dependent Cys113 nitrosylation. The protein (small domain in lighter blue), ATP, and glycine are shown as cartoon. Cys113, Lys114, and Asp318 on both subunits are highlighted. The figure was prepared with Inkscape version 0.92

higher than in the hSR<sup>MD</sup> medoid, partly due to the effect of Asp318, and partly due to its deeper buriedness (40% in chain A). Therefore, Asp318 can increase Cys113 pK<sub>a</sub> only in the closed conformation stabilized by glycine. To test the shielding of Cys113 by Asp318, we introduced the Asp318Ala and Asp318Asn virtual mutations in the hSR-Gly<sup>MD</sup> medoid. Cys113 pK<sub>a</sub> was predicted to be 9.70 and 9.86 in hSR-Gly<sup>Asp318Ala</sup> and hSR-Gly<sup>Asp318Asn</sup>, respectively, substantially lower than in the WT hSR-Gly<sup>MD</sup> medoid (11.11). This prediction is consistent with the experimentally observed higher reactivity of Cys113 in the glycine-bound conformation of these variants in comparison with glycine-bound WT hSR. The overall model that we propose is depicted in Fig. 9.

### Oxidation of Cys113 by H<sub>2</sub>O<sub>2</sub>

In the search for further physiological functions of the conformation-dependent reactivity of Cys113, we evaluated its oxidation by H<sub>2</sub>O<sub>2</sub>, which is produced at the NMDA synapsis, particularly under pathological

conditions [43]. Upon incubation with 1 mM H<sub>2</sub>O<sub>2</sub>, hSR underwent an 80% reduction in activity within 20 min (Fig. 10A), whereas Cys113Ser hSR was only 30% inactivated (Fig. 10A). This finding points to Cys113 as the target for H<sub>2</sub>O<sub>2</sub>-mediated oxidation. When glycine was also present, the reactivity of Cys113 decreased dramatically (Fig. 10B), suggesting a protective role of glycine associated with the same conformational equilibrium observed for the reactivity with GSNO. Cys113Ser variant showed the same level of inactivation even in the presence of both ATP and glycine, confirming the relevance of this residue for both S-nitrosylation and oxidation in hSR.

### Conclusion

The structural bases of the allosteric modulation of protein function by S-nitrosylation—one of the smallest post-translational modifications—are not entirely clear. Here, we showed that nitrosylation of a specific cysteine residue of hSR shifts its conformational equilibrium toward an open, less-active conformation, thus

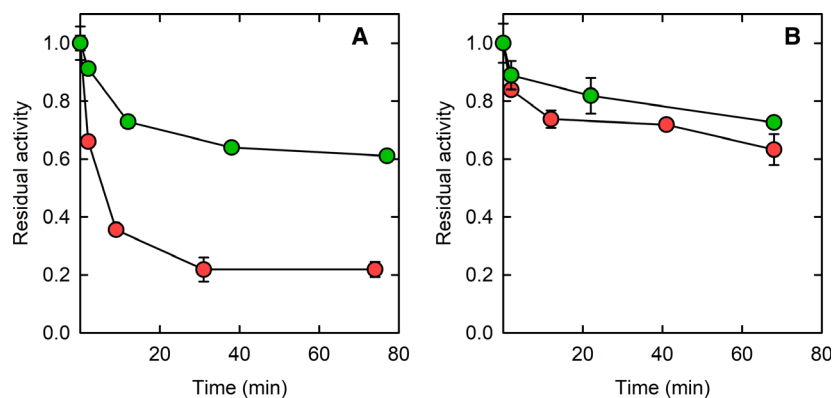


**Fig. 10.** Initial velocity of the  $\beta$ -elimination of L-serine (500 mM) by WT hSR (A) and Cys113Ser hSR (B) in the presence of ATP (6 mM) after addition of 1 mM  $\text{H}_2\text{O}_2$  in the absence (red circles), and presence of 1 mM glycine (green circles). The error bars are the S.E.M. of three independent experiments

reducing enzyme activity. ATP is required for nitrosylation as it stabilizes a conformation in which the thiol group of Cys113 is closer to the  $\epsilon$ -amino group of Lys114, confirming the need for at least one basic residue in the proximity of the reactive thiol, as observed in other proteins [44,45]. However, no acidic residue was shown to increase the nucleophilicity of Cys113. Glycine binding at the active site prevents S-nitrosylation through a conformational modification that involves Asp318. This modulation of hSR activity is particularly interesting, as glycine exhibits intracellular concentrations ranging from 2 mM in astrocytes [28] to 10 mM in glycinergic neurons [34]. In consideration of a measured  $K_D$  of 0.47 mM [11], a significant active-site occupancy of hSR by glycine is therefore expected.

We speculate that there are two mechanisms aimed at maintaining basic levels of D-serine production: i) at nonsaturating ATP concentrations, hSR cannot be further inhibited by nitrosylation, and ii) when glycine concentration increases and directly competes with L-serine at the active site, nitrosylation does not occur. The highest level of S-nitrosylation occurs for the maximally active form, that is, in the presence of ATP and in the absence of glycine, possibly to avoid overproduction of D-serine. A complex conformation-dependent nitrosylation has been observed so far only for hemoglobin [46] and a few other proteins [47,48].

Finally, Cys113 irreversible oxidation produced by ROS following NMDAR excitation might compete with reversible Cys nitrosylation, with a possible

protective effect suggested for other proteins at the glutamergic synapses [30,49], adding a further layer in the complexity of hSR allosteric regulation and to the homeostasis of D-serine.

## Materials and methods

### Materials

Chemicals were of the best commercial quality available and were purchased from Sigma-Aldrich (St. Louis, MO, USA) unless otherwise stated. Tris(2-carboxyethyl)phosphine (TCEP) was purchased from Apollo Scientific (Bredbury, UK).

### Site-directed mutagenesis and protein expression

Variants Asp318Ala, Asn316Ala, and Lys114Gln were obtained by site-directed mutagenesis of the plasmid encoding WT hSR [50] by the QuikChange protocol (Stratagene, San Diego, CA, USA) using the primers indicated in Table 3. In the case of the Asn316Ala mutation, a restriction site was also introduced (underlined in Table 3) to allow for faster identification of the mutated plasmid. The artificial gene encoding variant Cys2Ser, Cys4Ser, Cys128Ser, Cys269Ser, Cys309Ser ( $\Delta 5\text{Cys}$ ), codon-optimized for *Escherichia coli*, was synthesized by GeneArt (Regensburg, Germany) and subcloned in a pET28 expression vector. All variants were then expressed and purified as described for

**Table 3.** Primers used for site-directed mutagenesis

Mutations	Forward primer	Reverse primer
Asp318Ala	t c a g t g g t g g a a t g t a g c c t t a a c c t c t c c a t a a c	g t t a t g g a g g a g g t t a a g g c t a c a t t t c c a c c a c t g a
Asn316Ala	g c t c a g t g g t g g a g c t g t a g a t c t a a c c t c t c c a t a a c t t g g g	c c c a a g t t a t g g a g g a g g t t a g a t c t a c a g c t c c a c c a c t g a c
Lys114Gln	c c a g a c a g c t c c a g a c t g t c a g a a a c t t g c a a t a c a a g c c t	a g g c t t g t a t t g c a a g t t t c t g a c a g t c t g g a g c t g t c t g g
Glu276Gln	g t a g t t t c a t c c t c t g c c a c a c c a g c t g g g t	a c c a g c t g g t g t g g c a g a g g a t g a a a c t a c

WT hSR in *E. coli* BL21 CodonPlus (DE3)-RIL cells (Merck Millipore, Darmstadt, Germany) [11], co-expressing GroEL and GroES [40]. Mutagenesis, expression, and purification of variants Cys113Ser, Asp318Asn, and Gln89Met were reported previously [20,40].

### S-nitrosylation by GSNO

S-nitrosylation of WT hSR and its variants was produced by incubation with GSNO at concentrations ranging from 150 to 500  $\mu\text{M}$  for up to 90 min (as specified in each experiment), at 25 °C, in a buffered solution containing 50 mM triethanolamine (TEA), 150 mM NaCl, pH 8.0 in the presence of i) 6 mM adenosine triphosphate (ATP) and 10 mM  $\text{MgCl}_2$ , ii) 10 mM  $\text{MgCl}_2$ , iii) 0.5 to 80 mM glycine and 10 mM  $\text{MgCl}_2$ , iv) 5 mM ethylenediaminetetraacetic acid (EDTA). In reactions with GSNO, WT hSR or its variants were at concentrations of 0.5  $\mu\text{M}$  for the  $\beta$ -elimination assays, 4  $\mu\text{M}$  for the racemization assays and the fluorescence measurements, and 11  $\mu\text{M}$  for the in-gel S-nitrosylation detection and mass spectrometry experiments.

### S-nitrosylation by NO

S-nitrosylation of WT hSR by nitric oxide was produced by incubating WT hSR (4  $\mu\text{M}$ ) at 25 °C with 95  $\mu\text{M}$  of the NO donor (Z)-1-[N-methyl-N-[6-(N-methylammoniohexyl)amino]diazene-1-ium-1,2-diolate (MAHMA NONOate), which releases free NO with a  $t_{1/2}$  of 3 min in phosphate buffer. The solution of MAHMA NONOate was prepared anaerobically under a nitrogen atmosphere. S-nitrosylation of WT SR was performed using a modified tonometer [51] in a buffered solution containing 50 mM TEA, 150 mM NaCl, 10 mM  $\text{MgCl}_2$ , and 6 mM ATP, pH 8.0. The same experiment was carried out both under a nitrogen atmosphere and after exposing the sample to air.

### Oxidation of hSR by $\text{H}_2\text{O}_2$

Cysteine oxidation was produced upon incubation of WT and Cys113Ser hSR at a concentration of 4  $\mu\text{M}$  with 1 mM  $\text{H}_2\text{O}_2$  at 25 °C in a buffered solution containing 50 mM triethanolamine (TEA), 150 mM NaCl, pH 8.0.

### Activity assays

Activity assays for L-serine  $\beta$ -elimination [6,35] were carried out at 25 °C in a solution containing 50 mM TEA, 2 mM ATP, 500 mM L-serine, 50  $\mu\text{M}$  PLP, 2 mM  $\text{MgCl}_2$ , 150 mM NaCl, 60 U/ml lactate dehydrogenase (LDH), and 300  $\mu\text{M}$  NADH, at pH 8.0. The concentrations of L-serine, ATP, or  $\text{MgCl}_2$  were modified in some experiments, as specified. In some experiments, glycine was also added at 3 mM or 6 mM final concentration, as specified. For the

evaluation of GSNO inhibition, aliquots of the incubation mixtures were assayed for residual activity by adding 500 mM L-serine, 300  $\mu\text{M}$  NADH, and 60 U/ml LDH. It was preliminarily shown that LDH was not directly inhibited by GSNO (data not shown). GSNO was maintained in the assay mixtures at the same concentration as in the incubation mixtures to avoid dilution. All reactions were carried out at 25 °C. For the determination of enzyme parameters of hSR variants, the reactions were carried out at 37 °C and were triggered by the addition of the enzyme at a final concentration of 0.3–0.5  $\mu\text{M}$ .

Activity assays for the racemization of L-serine were performed as already described [35,52], in an assay mixture containing 50 mM TEA, 150 mM NaCl, 50 mM PLP, 6 mM ATP, and 4  $\mu\text{M}$  hSR, pH 8. The enzyme was assayed before and after 5 min incubation with 150  $\mu\text{M}$  GSNO. For some experiments, 1 mM glycine was also added to the reaction mixture, as specified. The reaction was triggered by the addition of 50 mM L-serine, and the mixtures were sampled over time. For each sample, the reaction was stopped by the addition of 200 mM  $\text{H}_3\text{PO}_4$  and the samples were treated with *Rhodotorula gracilis* DAAO (RgDAAO) and horseradish peroxidase (HRP) to estimate D-serine concentration [35,52]. Briefly, D-serine reacts with RgDAAO to give hydrogen peroxide, which then reacts with *o*-dianisidine in the presence of HRP. The absorbance of the chromophoric product after acidification with  $\text{H}_2\text{SO}_4$  was measured using a HALO LED 96 microplate reader (Dynamica) set at 550 nm.

### Fluorescence measurements

Fluorescence kinetic measurements of WT hSR and its variants were performed in the presence of 150  $\mu\text{M}$  GSNO, using a FluoroMax-3 fluorometer (HORIBA-Jobin Yvon), thermostatted at  $25.0 \pm 0.5$  °C. The solution contained 4  $\mu\text{M}$  hSR, 50 mM TEA, 150 mM NaCl, 6 mM ATP, and 10 mM  $\text{MgCl}_2$ , pH 8.0 in the absence and presence of glycine, from 0.5 mM to 80 mM as specified for each experiment. The fluorescence of PLP was excited at 445 nm, to avoid any inner filter effect from GSNO, which has an absorption peak centered at about 336 nm. Slits were set for optimal signal-to-noise ratio. Emission was collected at 490 nm when working in the absence of glycine and 482 nm when working in its presence [11]. Data points were collected with the shutter closed in-between to avoid photobleaching. Spectra were corrected for the buffer contribution.

### Detection of S-nitrosocysteines by differential tagging

Detection of S-nitrosylation was carried out using a differential tagging approach [53] with 5-iodoacetamidofluorescein and iodoacetamide (5-IAF switch technique). After

GSNO-induced nitrosylation for 90 min, unreacted cysteine residues were blocked through carbamidomethylation, using iodoacetamide (IAA) at 10 mM concentration at 50 °C. The products were then precipitated with 9 volumes of 96% ethanol at 80 °C for 30 min and extensively washed with pure ethanol to completely remove unreacted IAA. The pellets were resuspended in a buffer solution containing 50 mM TEA, 2 mM EDTA, 1% SDS, and 0.3 mM 5-iodoacetamide fluorescein (5-IAF) at pH 8.0. Finally, sodium ascorbate was added at 10 mM final concentration to reduce nitrosothiols [53] and the mixture was incubated at 25 °C in the dark for 2 h. Upon completion of the reaction, the excess of 5-IAF was removed through ice-cold precipitation with 1 volume of 10% trichloroacetic acid (TCA) and then extensively washed with pure acetone. The pellets were dried using a SpeedVac<sup>TM</sup> system, resuspended, and analyzed by SDS/PAGE. The gels were washed with water to remove SDS and fluorescence was detected using a Chemidoc system (Bio-Rad). The gels were then stained with Coomassie Blue. Coomassie staining allowed for the normalization of the fluorescence signals.

### Identification of S-nitrosylated cysteine residues

The bands corresponding to hSR in the same gels used for in-gel detection of fluorescence (see above) were excised, incubated with a solution containing 50% ethanol and 10% acetic acid until fully destained, washed twice with a buffered solution containing 25 mM ammonium bicarbonate and pure acetonitrile (ACN) 1:1 for 20 min and finally incubated with pure ACN for 5 min to reach complete dehydration. After removal of ACN, a solution containing trypsin in a 25 mM ammonium bicarbonate solution, pH 7.4, was added for gel rehydration. In-gel digestion was performed at 37 °C for 16 h. The reaction of trypsin was stopped by the addition of ACN: 0.1% trifluoroacetic acid (TFA) 1:1. Peptides were extracted by incubating the gel fragment with ACN: 0.1% TFA 1:1 twice for 20 min at 37 °C, before complete drying using a vacuum concentrator. The resulting pellets were resuspended with ACN:TFA 0.1% 1:1 before mass spectrometry experiments. Mass spectrometry on digested peptides was carried out using an LTQ-Orbitrap (Thermo Fisher Scientific) mass spectrometer. The peptide mixture was separated in a Phenomenex Aeris<sup>TM</sup> PEPTIDE 3.6 µm XB-C18 (150 mm × 2.1 mm) reverse-phase column, developed in a 0.2% formic acid/water-0.2% formic acid/acetonitrile gradient (200 µl/min). Peptide identification from LTQ-Orbitrap experiments was carried out using the software PEAKS Studio (version 8.5, Bioinformatics Solutions, Waterloo, Canada), set to a precursor mass tolerance of 10 ppm and a fragment mass error tolerance of 0.2 Da. The calculation of the AUC of the peaks conjugated with 5-IAF or IAA was performed using the software Xcalibur<sup>TM</sup> (Thermo Fisher Scientific).

## Molecular modeling

### hSR<sup>MD</sup> model

The hSR configuration corresponds to the homodimeric protein in the internal aldimine form, that is, the PLP group is covalently bound to Lys56. One ATP molecule and two Mg<sup>2+</sup> ions (one coordinated by ATP phosphate groups) are also present in each protomer. In the absence of a human SR structure complexed with ATP, the hSR model was built through a homology modeling procedure using the SWISS-MODEL web server [54]. The structure of *S. pombe* SR complexed with AMPPCP was used as a template (PDB code 1WTC [25]). In the obtained hSR model, the structure of AMPPCP was substituted by that of ATP. The available crystallographic structures of the open form of mammalian SRs in the absence of ATP (PDB codes 5X2I, 3HMK) exhibit a truncated or disordered C terminus, adjacent to Cys113, and were thus not considered for MD simulations.

### NOhSR<sup>MD</sup> model

The NOhSR configuration corresponds to the hSR one with the nitrosylated Cys113.

### hSR-Gly<sup>MD</sup> model

The hSR-Gly configuration corresponds to the homodimeric protein being in the external aldimine form, that is, the PLP group is covalently bound to the substrate or to an inhibitor. The PLP has been covalently bound to a glycine molecule. The glycine position has been retrieved from the crystal structure of S172AbsSHMT (PDB code 2vi9): the PLP group of 2vi9 and hSR model have been aligned and the glycine copied in hSR binding site. The glycine and the surrounding residues have been minimized with the conjugate-gradient scheme for a maximum of 1000 iterations, before submitting the system to the MD protocol.

### NOhSR-Gly<sup>MD</sup> model

The NOhSR-Gly configuration corresponds to the hSR-Gly one with the nitrosylated Cys113.

The stereochemical validation of the predicted model was carried out by building the Ramachandran plot of the protein-backbone structure using the RAMPAGE server (<http://mordred.bioc.cam.ac.uk/~rapper/rampage.php>). The hSR model, from which all the others were derived, presented 92.5% of the residues in favored regions, 5.3% in allowed regions, and 2.2% in outlier regions (Fig. S17). The last percentage decreased upon equilibration to 1.1%, and, as expected, all the models showed higher quality upon MD simulations. The extracted medoids for each model showed the following values.



hSR medoid: 94.3% residues in favored regions, 5.4% in allowed regions, 0.3% in outlier regions (Fig. S18a).

hSR-NO medoid: 94.4% residues in favored regions, 5.3% in allowed regions, 0.3% in outlier regions (Fig. S18b).

hSR-Gly medoid: 94.3% residues in favored regions, 4.9% in allowed regions, 0.8% in outlier regions (Fig. S18c).

hSR-GlyNO medoid: 94.1% residues in favored regions, 5.2% in allowed regions, 0.6% in outlier regions (Fig. S18d).

### Nonstandard residue parameterization

To perform MD simulations, the force field parameters of N'-pyridoxyl-lysine-5'-monophosphate (KPLP) were derived and implemented into the Amber-ILDN force field libraries, following previous protocols [55–58] and described below. The force constants were assigned taking into account the analogous values in standard amino acid fragments as included in the Amber-ILDN force field library. Those corresponding to the lysine main and side chains connected to pyridoxyl-5'-monophosphate were extracted from the force field data. The atomic charges of the full KPLP residue were obtained using the RESP ESP charge Derive (pyR.E.D.) server [59], by following the standard protocol proposed by Cornell *et al.* [60]. The S-nitrosocysteine was parameterized using the data derived and validated by Han [61]. The glycine in the external aldimine form and the ATP was parameterized using the *ab initio* RESP-charge-fitting methodology, as implemented in the BiKi Life Science software suite (<http://www.bikitech.com>; [62]), and converted into GROMACS format with the acypipe tool.

### Molecular dynamics simulations

Simulations were run with GROMACS 4.6.1 [63] in an octahedron box solvated using the TIP3P water models [64] with a 1.2 nm distance to the border of the molecule. Ions were added to reach neutrality. Periodic boundary conditions were employed; the LINCS algorithm [65] was used to constrain all bond lengths. An integration time step of 2 fs was used. Particle mesh Ewald method was used to treat electrostatics, a nonbonded cutoff of 1.4 nm was applied for the Lennard–Jones potential. NPT conditions (298 K and 1 bar) were used to run the simulation and the Berendsen algorithm for temperature and pressure control, with a coupling constant of 5 ps for both. Water molecules were relaxed by energy minimization and followed by 10 ps MD at 298 K, harmonically restraining the atomic positions. The systems were heated up gradually to 298 K in a six-step process, from 50 K to 298 K. In particular, 6 equilibrations of 15 ps each were performed in NPT, followed by a short 5 ps-long equilibration at 298 K at NPT. The

production was run in NPT standard conditions, without restraints, for 1  $\mu$ s.

The analyses of the MD trajectories were done by the GROMACS package [66,67], images were generated with PyMOL (Schrodinger, LLC, 2010. The PyMOL Molecular Graphics System, version 2.3.4) and Chimera version 1.14 [68]. Essential dynamics (ED), also known as principal component analysis (PCA), was carried out to reduce the multidimensionality of protein motion to an essential subspace. First, roto-translations were removed; then, the covariance matrix was calculated and diagonalized, and lastly, the first 10 eigenvectors were extracted and sorted out in descending order, depending on their eigenvalue. The first and the second eigenvectors were selected as the *x*-axis and *y*-axis, respectively, describing the essential space in PCA plots. Network analysis was carried out with RINalyzer [69] in Cytoscape 3.1 version [70]. Plots were generated in MATLAB (MATLAB, 2018, Natick, Massachusetts, USA). The DynDom SelectDomain program was used to calculate rotation between the small domain (as the moving domain) and the large domain (as the fixed domain) in medoids [42]. PROPKA 3.0 [71] was used to predict Cys113 pK<sub>a</sub> with an empirical method.

### Data analysis

Graphical and statistical analyses were performed with the software SigmaPlot (Systat Software, San Jose, CA, USA).

The  $V_{\max}$  and  $K_M$  of WT hSR and its variants were determined by fitting the dependence of activity on L-serine concentration with eq. 1:

$$v = \frac{V_{\max}[S]}{K_M + [S]} \quad (1)$$

where  $v$  is the reaction velocity,  $V_{\max}$  is the maximal velocity at saturating concentrations of substrate,  $[S]$  is the concentration of the substrate, and  $K_M$  is the Michaelis–Menten constant.

The analysis of the GSNO-mediated inactivation kinetics and fluorescence changes of WT hSR and variants were carried out under the assumption of a pseudo-first-order kinetic at high GSNO concentrations [72] using a sum of two exponential decays, plus a baseline to account for the residual activity or the residual fluorescence:

$$A = A_0 + a_1 e^{-[GSNO]k_1 t} + a_2 e^{-[GSNO]k_2 t} \quad (2)$$

where  $A$  is the enzyme activity or the fluorescence emission;  $A_0$  is the residual activity or the residual fluorescence;  $a_1$  and  $a_2$  the amplitudes of the two inhibition phases;  $k_1$  and  $k_2$  are the second-order rate constants.

The analysis of the GSNO inactivation kinetics for the variants that did not exhibit a biphasic behavior was carried out under the assumption of a pseudo-first-order

kinetic at high GSNO concentrations [72] using a single exponential decay, plus a baseline to account for the residual activity or the residual fluorescence:

$$A = A_0 + ae^{-[GSNO]kt} \quad (3)$$

where  $A$  is the enzyme activity or the fluorescence emission,  $A_0$  the residual activity or the residual fluorescence,  $a$  the amplitude of the inhibition time course, and  $k$  the reaction rate constant.

For the analysis of the dependence of fluorescence emission or enzyme activity on ATP concentration, a sigmoidal equation was used to take into account the binding cooperativity [11].

$$y = y_0 + a \frac{[ATP]^n}{K_D^n + [ATP]^n} \quad (4)$$

where  $y$  is the fluorescence emission intensity or the enzyme velocity,  $[ATP]$  is the ligand concentration, and  $n$  is the Hill coefficient.  $y_0$  is a horizontal offset and  $a$  the amplitude.

For the analysis of the  $K_{50}$  of glycine obtained with enzyme assay or fluorescence experiments as a function of glycine concentrations, a hyperbolic equation was used:

$$y = a \frac{[Gly]}{K_{50} + [Gly]} \quad (5)$$

where  $y$  represents the rate constants,  $[Gly]$  is the glycine concentration, and  $a$  is the amplitude.

## Acknowledgments

We kindly thank the Centro di Competenza sul Calcolo Scientifico (C3S) of the University of Turin for providing the computational time and resources and BiKi technologies for providing the BiKi Life Sciences suite.

## Conflicts of interest

The authors declare no conflict of interest.

## Author contributions

SB and FS conceived the study, designed the experiments, analyzed the results, and wrote the manuscript. FM and AMi performed the experiments. EG performed the computational simulations, analyzed the results, and wrote part of the manuscript. IA performed the computational parameterization. SB, FS, EG, FM, AMo, BC, SF, and SB interpreted the data. AMo, BC, SF, and SB reviewed and edited the manuscript.

## Peer Review

The peer review history for this article is available at <https://publons.com/publon/10.1111/febs.15645>.

## References

- Hess DT, Matsumoto A, Kim SO, Marshall HE & Stamler JS (2005) Protein S-nitrosylation: purview and parameters. *Nat Rev Mol Cell Biol.* **6**, 150–166.
- Broniowska KA, Diers AR & Hogg N (2013) S-nitrosoglutathione. *Biochim Biophys Acta.* **1830**, 3173–3181.
- Jia J, Arif A, Terenzi F, Willard B, Plow EF, Hazen SL & Fox PL (2014) Target-selective protein S-nitrosylation by sequence motif recognition. *Cell* **159**, 623–634.
- Wolosker H, Blackshaw S & Snyder SH (1999) Serine racemase: a glial enzyme synthesizing D-serine to regulate glutamate-N-methyl-D-aspartate neurotransmission. *Proc Natl Acad Sci U S A.* **96**, 13409–13414.
- De Miranda J, Panizzutti R, Foltyn VN & Wolosker H (2002) Cofactors of serine racemase that physiologically stimulate the synthesis of the N-methyl-D-aspartate (NMDA) receptor coagonist D-serine. *Proc Natl Acad Sci U S A.* **99**, 14542–14547.
- Foltyn VN, Bendikov I, De Miranda J, Panizzutti R, Dumin E, Shleper M, Li P, Toney MD, Kartvelishvili E & Wolosker H (2005) Serine racemase modulates intracellular D-serine levels through an alpha, beta-elimination activity. *J Biol Chem.* **280**, 1754–1763.
- Foltyn VN, Zehl M, Dikopoltsev E, Jensen ON & Wolosker H (2010) Phosphorylation of mouse serine racemase regulates D-serine synthesis. *FEBS Lett* **584**, 2937–2941.
- Hoffman HE, Jiraskova J, Cigler P, Sanda M, Schraml J & Konvalinka J (2009) Hydroxamic acids as a novel family of serine racemase inhibitors: mechanistic analysis reveals different modes of interaction with the pyridoxal-5'-phosphate cofactor. *J Med Chem.* **52**, 6032–6041.
- Campanini B, Spyraakis F, Peracchi A & Mozzarelli A (2013) Serine racemase: a key player in neuron activity and in neuropathologies. *Front Biosci.* **18**, 1112–1128.
- Canu N, Ciotti MT & Pollegioni L (2014) Serine racemase: a key player in apoptosis and necrosis. *Frontiers in synaptic neuroscience.* **6**, 9.
- Marchetti M, Bruno S, Campanini B, Peracchi A, Mai N & Mozzarelli A (2013) ATP binding to human serine racemase is cooperative and modulated by glycine. *FEBS J.* **280**, 5853–5863.
- Raboni S, Marchetti M, Faggiano S, Campanini B, Bruno S, Marchesani F, Margiotta M & Mozzarelli A (2018) *The energy landscape of human serine racemase, frontiers in molecular biosciences.* **5**, 112.

- 13 Ohshima K, Nojima S, Tahara S, Kurashige M, Kawasaki K, Hori Y, Taniguchi M, Umakoshi Y, Okuzaki D, Wada N *et al.* (2020) Serine racemase enhances growth of colorectal cancer by producing pyruvate from serine. *Nature Metabolism*. **2**, 81–96.
- 14 Dellafiora L, Marchetti M, Spyrikis F, Orlandi V, Campanini B, Cruciani G, Cozzini P & Mozzarelli A (2015) Expanding the chemical space of human serine racemase inhibitors. *Bioorg Med Chem Lett*. **25**, 4297–4303.
- 15 Wolosker H, Sheth KN, Takahashi M, Mothet JP, Brady RO Jr, Ferris CD & Snyder SH (1999) Purification of serine racemase: biosynthesis of the neuromodulator D-serine. *Proc Natl Acad Sci U S A*. **96**, 721–725.
- 16 Wolosker H, Balu DT & Coyle JT (2016) The rise and fall of the d-serine-mediated gliotransmission hypothesis. *Trends Neurosci*. **39**, 712–721.
- 17 Martinez-Ruiz A, Araujo IM, Izquierdo-Alvarez A, Hernansanz-Agustin P, Lamas S & Serrador JM (2013) Specificity in S-nitrosylation: a short-range mechanism for NO signaling? *Antioxid Redox Signal*. **19**, 1220–1235.
- 18 Shoji K, Mariotto S, Ciampa AR & Suzuki H (2006) Regulation of serine racemase activity by D-serine and nitric oxide in human glioblastoma cells. *Neurosci Lett*. **392**, 75–78.
- 19 Mustafa AK, Kumar M, Selvakumar B, Ho GP, Ehmsen JT, Barrow RK, Amzel LM & Snyder SH (2007) Nitric oxide S-nitrosylates serine racemase, mediating feedback inhibition of D-serine formation. *Proc Natl Acad Sci U S A*. **104**, 2950–2955.
- 20 Marchesani F, Bruno S, Paredi G, Raboni S, Campanini B & Mozzarelli A (2018) Human serine racemase is nitrosylated at multiple sites. *Biochim Biophys Acta*. **1866**, 813–821.
- 21 Sossa KG, Beattie JB & Carroll RC (2007) AMPAR exocytosis through NO modulation of PICK1. *Neuropharmacology* **53**, 92–100.
- 22 Padgett CM & Whorton AR (1995) S-nitrosoglutathione reversibly inhibits GAPDH by S-nitrosylation. *Am J Physiol*. **269**, C739–C749.
- 23 Choi YB, Tennen L, Le DA, Ortiz J, Bai G, Chen HS & Lipton SA (2000) Molecular basis of NMDA receptor-coupled ion channel modulation by S-nitrosylation. *Nat Neurosci*. **3**, 15–21.
- 24 Selvakumar B, Jenkins MA, Hussain NK, Haganir RL, Traynelis SF & Snyder SH (2013) S-nitrosylation of AMPA receptor GluA1 regulates phosphorylation, single-channel conductance, and endocytosis. *Proc Natl Acad Sci U S A*. **110**, 1077–1082.
- 25 Goto M, Yamauchi T, Kamiya N, Miyahara I, Yoshimura T, Mihara H, Kurihara T, Hirotsu K & Esaki N (2009) Crystal structure of a homolog of mammalian serine racemase from *Schizosaccharomyces pombe*. *J Biol Chem*. **284**, 25944–25952.
- 26 Huang H, Zhang X, Li S, Liu N, Lian W, McDowell E, Zhou P, Zhao C, Guo H, Zhang C *et al.* (2010) Physiological levels of ATP negatively regulate proteasome function. *Cell Res*. **20**, 1372–1385.
- 27 Dunlop DS & Neidle A (2005) Regulation of serine racemase activity by amino acids. *Brain Res Mol Brain Res*. **133**, 208–214.
- 28 Berger SJ, Carter JC & Lowry OH (1977) The distribution of glycine, GABA, glutamate and aspartate in rabbit spinal cord, cerebellum and hippocampus. *J Neurochem*. **28**, 149–158.
- 29 Neame S, Safory H, Radziszewsky I, Touitou A, Marchesani F, Marchetti M, Kellner S, Berlin S, Foltyn VN, Engelender S *et al.* (2019) The NMDA receptor activation by d-serine and glycine is controlled by an astrocytic Phgdh-dependent serine shuttle. *Proc Natl Acad Sci U S A*. **116**, 20736–20742.
- 30 Weinberg JM, Bienholz A & Venkatachalam MA (2016) The role of glycine in regulated cell death. *Cell Mol Life Sci*. **73**, 2285–2308.
- 31 Yamauchi T, Goto M, Wu HY, Uo T, Yoshimura T, Mihara H, Kurihara T, Miyahara I, Hirotsu K & Esaki N (2009) Serine racemase with catalytically active lysinoalanyl residue. *J Biochem*. **145**, 421–424.
- 32 Takahara S, Nakagawa K, Uchiyama T, Yoshida T, Matsumoto K, Kawasumi Y, Mizuguchi M, Obita T, Watanabe Y, Hayakawa D *et al.* (2017) Design, synthesis, and evaluation of novel inhibitors for wild-type human serine racemase. *Bioorg Med Chem Lett*.
- 33 Smith MA, Mack V, Ebneith A, Moraes I, Felicetti B, Wood M, Schonfeld D, Mather O, Cesura A & Barker J (2010) The structure of mammalian serine racemase: evidence for conformational changes upon inhibitor binding. *J Biol Chem*. **285**, 12873–12881.
- 34 Ottersen OP, Storm-Mathisen J, Bramham C, Torp R, Laake J & Gundersen V (1990) A quantitative electron microscopic immunocytochemical study of the distribution and synaptic handling of glutamate in rat hippocampus. *Prog Brain Res*. **83**, 99–114.
- 35 Marchetti M, Bruno S, Campanini B, Bettati S, Peracchi A & Mozzarelli A (2015) Regulation of human serine racemase activity and dynamics by halides. *ATP and malonate, Amino Acids*. **47**, 163–173.
- 36 Bruno S, Margiotta M, Marchesani F, Paredi G, Orlandi V, Faggiano S, Ronda L, Campanini B & Mozzarelli A (2017) Magnesium and calcium ions differentially affect human serine racemase activity and modulate its quaternary equilibrium toward a tetrameric form. *Biochim Biophys Acta*. **1865**, 381–387.
- 37 Cook SP, Galve-Roperh I, Martinez del Pozo A & Rodriguez-Crespo I (2002) Direct calcium binding results in activation of brain serine racemase. *J Biol Chem*. **277**, 27782–27792.
- 38 Ito T, Koga K, Hemmi H & Yoshimura T (2012) Role of zinc ion for catalytic activity in d-serine

- dehydratase from *Saccharomyces cerevisiae*. *FEBS J.* **279**, 612–624.
- 39 Lee RA, Razaz M & Hayward S (2003) The DynDom database of protein domain motions. *Bioinformatics* **19**, 1290–1291.
- 40 Canosa AV, Faggiano S, Marchetti M, Armao S, Bettati S, Bruno S, Percudani R, Campanini B & Mozzarelli A (2018) Glutamine 89 is a key residue in the allosteric modulation of human serine racemase activity by ATP. *Sci Rep* **8**, 9016.
- 41 Nelson DL, Applegate GA, Beio ML, Graham DL & Berkowitz DB (2017) Human serine racemase structure/activity relationship studies provide mechanistic insight and point to position 84 as a hot spot for beta-elimination function. *J Biol Chem.* **292**, 13986–14002.
- 42 Veevers R & Hayward S (2019) Methodological improvements for the analysis of domain movements in large biomolecular complexes. *Biophysics and physcobiology.* **16**, 328–336.
- 43 Garthwaite J (2008) Concepts of neural nitric oxide-mediated transmission. *Eur J Neurosci.* **27**, 2783–2802.
- 44 Greco TM, Hodara R, Parastatidis I, Heijnen HF, Dennehy MK, Liebler DC & Ischiropoulos H (2006) Identification of S-nitrosylation motifs by site-specific mapping of the S-nitrosocysteine proteome in human vascular smooth muscle cells. *Proc Natl Acad Sci U S A.* **103**, 7420–7425.
- 45 Perez-Mato I, Castro C, Ruiz FA, Corrales FJ & Mato JM (1999) Methionine adenosyltransferase S-nitrosylation is regulated by the basic and acidic amino acids surrounding the target thiol. *J Biol Chem.* **274**, 17075–17079.
- 46 Stamler JS, Singel DJ & Piantadosi CA (2008) SNO-hemoglobin and hypoxic vasodilation. *Nat Med.* **14**, 1008–1009. author reply 1009–10.
- 47 Lai TS, Hausladen A, Slaughter TF, Eu JP, Stamler JS & Greenberg CS (2001) Calcium regulates S-nitrosylation, denitrosylation, and activity of tissue transglutaminase. *Biochemistry* **40**, 4904–4910.
- 48 Eu JP, Sun J, Xu L, Stamler JS & Meissner G (2000) The skeletal muscle calcium release channel: coupled O<sub>2</sub> sensor and NO signaling functions. *Cell* **102**, 499–509.
- 49 Nakamura T, Prikhodko OA, Pirie E, Nagar S, Akhtar MW, Oh CK, McKercher SR, Ambasudhan R, Okamoto S & Lipton SA (2015) Aberrant protein S-nitrosylation contributes to the pathophysiology of neurodegenerative diseases. *Neurobiol Dis.* **84**, 99–108.
- 50 Dixon SM, Li P, Liu R, Wolosker H, Lam KS, Kurth MJ & Toney MD (2006) Slow-binding human serine racemase inhibitors from high-throughput screening of combinatorial libraries. *J Med Chem.* **49**, 2388–2397.
- 51 Ronda L, Bruno S, Faggiano S, Bettati S & Mozzarelli A (2008) Oxygen binding to heme proteins in solution, encapsulated in silica gels, and in the crystalline state. *Methods Enzymol.* **437**, 311–328.
- 52 Molla G, Piubelli L, Volonte F & Pilone MS (2012) Enzymatic detection of D-amino acids. *Methods Mol Biol.* **794**, 273–289.
- 53 Devarie-Baez NO, Zhang D, Li S, Whorton AR & Xian M (2013) Direct methods for detection of protein S-nitrosylation. *Methods* **62**, 171–176.
- 54 Waterhouse A, Bertoni M, Bienert S, Studer G, Tauriello G, Gumienny R, Heer FT, de Beer TAP, Rempfer C, Bordoli L *et al.* (2018) SWISS-MODEL: homology modelling of protein structures and complexes. *Nucleic Acids Res.* **46**, W296–W303.
- 55 Autiero I, Saviano M & Langella E (2015) Conformational studies of chiral D-Lys-PNA and achiral PNA system in binding with DNA or RNA through a molecular dynamics approach. *Eur J Med Chem.* **91**, 109–117.
- 56 Autiero I, Saviano M & Langella E (2014) Molecular dynamics simulations of PNA-PNA and PNA-DNA duplexes by the use of new parameters implemented in the GROMACS package: a conformational and dynamics study. *Phys Chem Chem Phys.* **16**, 1868–1874.
- 57 Piacenti V, Langella E, Autiero I, Nolan JC, Piskareva O, Adamo MFA, Saviano M & Moccia M (2019) A combined experimental and computational study on peptide nucleic acid (PNA) analogues of tumor suppressive miRNA-34a. *Bioorg Chem.* **91**, 103165.
- 58 Chawla M, Autiero I, Oliva R & Cavallo L (2018) Energetics and dynamics of the non-natural fluorescent 4AP:DAP base pair. *Phys Chem Chem Phys.* **20**, 3699–3709.
- 59 Vanquelef E, Simon S, Marquant G, Garcia E, Klimerak G, Delepine JC, Cieplak P & Dupradeau FY (2011) R.E.D. Server: a web service for deriving RESP and ESP charges and building force field libraries for new molecules and molecular fragments. *Nucleic Acids Res.* **39**, W511–W517.
- 60 Cornell WD, Cieplak P, Bayly CI, Gould IR, Merz KM, Ferguson DM, Spellmeyer DC, Fox T, Caldwell JW & Kollman PA (1995) A second generation force field for the simulation of proteins, nucleic acids, and organic molecules. *J Am Chem Soc.* **117**, 5179–5197.
- 61 Han S (2008) Force field parameters for S-nitrosocysteine and molecular dynamics simulations of S-nitrosated thioredoxin. *Biochem Biophys Res Commun.* **377**, 612–616.
- 62 Sciabola S, Benedetti P, D'Arrigo G, Torella R, Baroni M, Cruciani G & Spyraakis F (2019) Discovering New Casein Kinase 1d Inhibitors with an Innovative Molecular Dynamics Enabled Virtual Screening Workflow. *ACS medicinal chemistry letters.* **10**, 487–492.
- 63 Hess B, Kutzner C, van der Spoel D & Lindahl E (2008) GROMACS 4: Algorithms for Highly Efficient, Load-Balanced, and Scalable Molecular Simulation. *J Chem Theory Comput.* **4**, 435–447.



- 64 Mark P & Nilsson L (2001) Structure and Dynamics of the TIP3P, SPC, and SPC/E Water Models at 298 K. *The Journal of Physical Chemistry A*. **105**, 9954–9960.
- 65 Hess B, Bekker H, Berendsen H & Fraaije J (1998) LINCS: A Linear Constraint Solver for molecular simulations. *J Comput Chem*. **18**.
- 66 Barone D, Balasco N, Autiero I & Vitagliano L (2017) The dynamic properties of the Hepatitis C Virus E2 envelope protein unraveled by molecular dynamics. *J Biomol Struct Dyn*. **35**, 805–816.
- 67 Autiero I, Ruvo M, Improta R & Vitagliano L (2018) The intrinsic flexibility of the aptamer targeting the ribosomal protein S8 is a key factor for the molecular recognition. *Biochim Biophys Acta, Gen Subj*. **1862**, 1006–1016.
- 68 Pettersen EF, Goddard TD, Huang CC, Couch GS, Greenblatt DM, Meng EC & Ferrin TE (2004) UCSF Chimera—a visualization system for exploratory research and analysis. *J Comput Chem*. **25**, 1605–1612.
- 69 Doncheva NT, Klein K, Domingues FS & Albrecht M (2011) Analyzing and visualizing residue networks of protein structures. *Trends Biochem Sci*. **36**, 179–182.
- 70 Shannon P, Markiel A, Ozier O, Baliga NS, Wang JT, Ramage D, Amin N, Schwikowski B & Ideker T (2003) Cytoscape: a software environment for integrated models of biomolecular interaction networks. *Genome Res*. **13**, 2498–2504.
- 71 Olsson MH, Sondergaard CR, Rostkowski M & Jensen JH (2011) PROPKA3: Consistent Treatment of Internal and Surface Residues in Empirical pKa Predictions. *J Chem Theory Comput*. **7**, 525–537.
- 72 Rossi R, Lusini L, Giannerini F, Giustarini D, Lungarella G & Di Simplicio P (1997) A method to study kinetics of transnitrosation with nitrosoglutathione: reactions with hemoglobin and other thiols. *Anal Biochem*. **254**, 215–220.
- Fig. S2.** Fluoresce of SR in different ligation states.  
**Fig. S3.** Correlation between nitrosylation rates monitored in fluorescence and through enzyme assays.  
**Fig. S4.** Root Mean Square Deviation (RMSD) plots.  
**Fig. S5.** Principal component analysis (PCA) plots.  
**Fig. S6.** Gyration radius plot.  
**Fig. S7.** Human SR secondary structure.  
**Fig. S8.** RMSD matrices.  
**Fig. S9.** SSGNH segment reorganization in hSR upon ligand binding.  
**Fig. S10.** Residue interaction network of representative structures from MD simulations.  
**Fig. S11.** Fluorescence properties of the Asn316Ala variant.  
**Fig. S12.** Nitrosylation of hSR variants monitored by fluorescence.  
**Fig. S13.** Nitrosylation Asp318 hSR variants monitored by fluorescence.  
**Fig. S14.** Distances (Å) between the nitrogen of Lys114 and sulfur of Cys113.  
**Fig. S15.** Distances (Å) between the nitrogen of Lys114 and oxygen of the nitroso group of nitrosylated Cys113.  
**Fig. S15.** Distances (Å) between the nitrogen of Lys114 and oxygen of the nitroso group of nitrosylated Cys113.  
**Fig. S16.** Distances (Å) between the sulfur of Cys113 and the centre of mass of Asp318 carboxylic oxygens.  
**Fig. S17.** Ramachandran plot for the hSR<sup>MD</sup> model.  
**Fig. S18.** Ramachandran plot for the medoids extracted from the MD trajectories.  
**Table S1.** Nitrosylation rates of hSR monitored through fluorescence and enzyme assays.  
**Table S2.** Mass spectrometry of hSR  
**Table S3.** Average backbone RMSD and Standard Deviation calculated for all trajectories.  
**Table S4.** Radius of Gyration  $R_g$  (nm) averages and standard deviation.  
**Table S5.** Clustering results for MD trajectories.  
**Table S6.** DynDom analysis.

## Supporting information

Additional supporting information may be found online in the Supporting Information section at the end of the article.

**Fig. S1.** Effect of nitrosylation on  $\beta$ -elimination activity in the absence and presence of malonate.